

CONDITIONAL CO-ABLATION: RECOVERING SELF-REPAIR BACKUPS IN TRANSFORMER CIRCUITS

Zhiren Gong^{1,2} Zihao Zeng¹ Chau Yuen³ Wei Yang Bryan Lim¹

¹College of Computing and Data Science, Nanyang Technological University, Singapore

²Interdisciplinary Graduate Programme, Nanyang Technological University, Singapore

³School of Electrical and Electronic Engineering, Nanyang Technological University, Singapore
zhiren001@e.ntu.edu.sg bryan.limwy@ntu.edu.sg



Code



Project Page



Tutorial

ABSTRACT

Mechanistic interpretability often relies on component-level interventions to discover how a model produces a behavior. This guides attribution, capability knockout, and model pruning downstream to operate by scoring *each* unit by the effect of ablation in isolation. Such first-order scoring is natural when component importance is additive, but becomes misleading when a transformer *self-repairs*: after a primary component is removed, a dormant backup can take over, muting the primary’s measured effect while the backup itself appears irrelevant on the intact model. We recast this failure as a recovery task, *conditional circuit completion*, and introduce *conditional co-ablation* (COAX), a label-free, output-grounded score that asks how much each remaining unit’s ablation effect grows once a primary set has been removed. This conditional growth exposes the second-order interaction that single-unit scores discard. On the GPT-2-small IOI circuit, COAX raises backup-head recovery from 0.33 to 0.91 ROC-AUC, outperforming all baselines, including self-repair-aware gradient scores (best 0.82); counterfactual patching verifies that the recovered heads causally carry the repair. The same label-free procedure transfers to induction across eight models. Beyond discovery, the recovered backups correct self-repair-masked attribution, identify the components required for capability knockout, and yield repair-aware structured pruning scaling from 124M to 7B. Component importance is therefore not merely an isolated-unit property: in robust circuits, the components that matter can become visible only under the interventions that make them necessary.

1 INTRODUCTION

Understanding how a language model produces a behavior is central to auditing, debugging, and trusting it (Bereska & Gavves, 2024). A common strategy in mechanistic interpretability is to localize a behavior to a *circuit*: a small set of components that carries out the relevant computation (Elhage et al., 2021; Olah et al., 2020). This strategy depends on a basic primitive: assigning importance to individual components. The same primitive underlies automated circuit discovery (Wang et al., 2022; Conmy et al., 2023), feature attribution (Syed et al., 2023; Kramár et al., 2024), and structured pruning (Kwon et al., 2022; Sun et al., 2023). In many such methods, importance is estimated in a first-order way: ablate a unit in isolation, measure the output change, and combine these single-unit effects across the circuit. Attribution and edge patching, EAP-IG (Sundararajan et al., 2017; Hanna et al., 2024), AtP* (Kramár et al., 2024), sparse feature circuits (Marks et al., 2024), and Wanda saliency (Sun et al., 2023) all rely, in different forms, on this node-additive view.

This view is natural when components contribute independently, but self-repair shows where it can fail. In the Hydra effect (McGrath et al., 2023; Rushing & Nanda, 2024), removing a primary component can activate a dormant *backup* that substitutes for it. The primary then appears less important than it is, because the model repairs the damage; the backup also appears unimportant, because it is largely silent on the intact model. A first-order score therefore misreads both sides of the redundancy. In GPT-2-small IOI, for example, ablating the name-mover heads that write the answer reduces the task logit-difference by only 0.22 from a clean value of 2.53, because backup

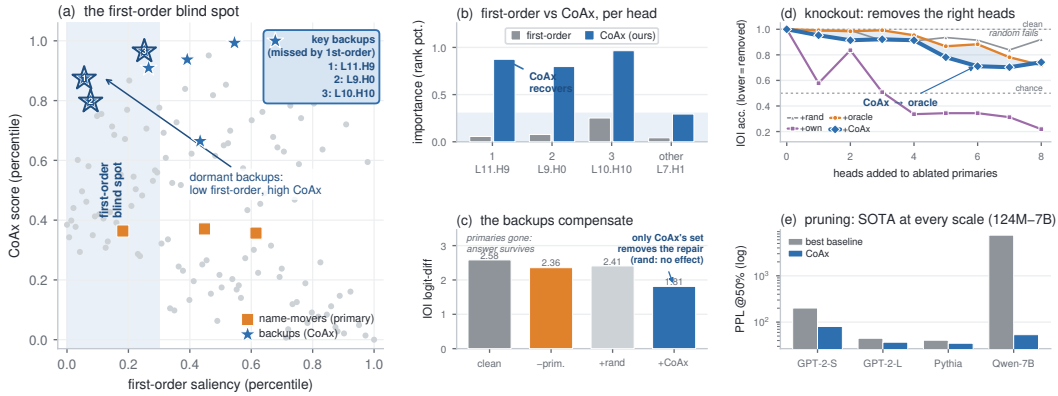


Figure 1: **COAX exposes the self-repair backups first-order scoring misses, and the same score pays off downstream** on GPT-2-small. (a) The documented backups sit in the *first-order blind spot*, lifting backup ROC-AUC 0.33 \rightarrow 0.91. (b) First-order leaves the key backups in the blind spot while COAX ranks them at the top, whereas an inactive head stays low under both. (c) Ablating the primaries barely moves the IOI answer margin (the backups take over), and only ablating the backups too collapses it. (d) Knockout: COAX-ordered additions drive IOI accuracy to the documented oracle (lower = more removed), while a first-order top-up (+own) overshoots and a random one fails to move it. (e) Pruning: at 50% sparsity COAX beats the best competing baseline at every scale from 124M to 7B (full sweep, Figure 5). Attribution and generalization: Section 4, Figure 4.

name-movers take over. The larger effect appears only when the backups are removed as well. This is not a noisy measurement artifact but rather a violation of additivity: the IOI name-mover module is $1.9\times$ super-additive, so the effect of removing a set is not the sum of the effects of removing its members. The resulting bias falls exactly on the redundant components that make a circuit robust and therefore propagates to attribution, knockout, and pruning downstream.

We therefore ask a conditional question: not how much a unit matters on the intact model, but how much it matters once the primary circuit has been removed. Given a candidate primary set S , we measure how much each remaining unit’s output effect *grows* under that intervention. A dormant backup has little effect alone but a large conditional effect; an irrelevant unit has neither. This reframing is substantive, not merely procedural: importance stops being an intrinsic property a unit carries and becomes a quantity defined relative to what has been removed, the only frame in which a component that stays silent until its primary fails can be said to matter at all. We call this score COAX, for *conditional co-ablation*. It is label-free and output-grounded: it measures growth in Fisher-weighted ablation energy using a single-ablation baseline and one conditional pass. Conceptually, COAX reads the second-order interaction that node-additive scores discard. Operationally, it solves *conditional circuit completion*: given a primary circuit found by manual analysis or a first-order method, recover the components that become causal only when that circuit is removed. Thus COAX complements first-order discovery rather than replacing it.

Empirically, on the labeled GPT-2-small IOI circuit (Wang et al., 2022), COAX raises backup-head identification from 0.33 to 0.91 ROC-AUC, outperforming baselines including self-repair-aware AtP* GradDrop (best 0.82). Counterfactual patching confirms that the recovered heads causally carry the repair. The same label-free procedure transfers to induction across eight models. Once recovered, the backups also close the downstream loop: they restore a much larger self-repair-masked attribution signal (1.76 versus 0.22 logit-difference drop), identify the components required for capability knockout (0.70 accuracy, matching the 0.72 documented oracle), and improve structured head pruning, scaling from 124M to 7B. In short, first-order methods find the circuit a model uses when everything is intact; COAX exposes the circuit it falls back on when that path is removed.

Contributions. (i) Conditional component importance. We formalize self-repair as an additivity failure of component importance, introduce conditional circuit completion, and propose COAX, a label-free, Fisher-grounded score for recovering dormant compensators (Section 2). **(ii) Causal validation of recovered backups.** We validate COAX on the documented GPT-2 IOI backup heads, a controlled-redundancy benchmark, mechanistic patching, and faithfulness/completeness checks,

and show label-free transfer to induction across eight models in six architecture families (Section 3). **(iii) Downstream closure.** We show that the recovered backups correct self-repair-masked attribution, scope capability knockout, and yield repair-aware structured pruning (Section 4).

2 CONDITIONAL CO-ABLATION: EXPOSING NON-ADDITIVE IMPORTANCE

We study frozen decoder-only transformers. A *structured unit* u is any component with an additive residual-stream contribution that ablation can zero (Elhage et al., 2021); COAX is unit-agnostic, and our main experiments use attention heads, the granularity at which head-level circuit ground truth exists. Ablating a set M of units replaces their contributions with zero and yields logits z_M over the vocabulary at a given position, with $z_\emptyset \equiv z_0$ the clean logit vector and $p_0 = \text{softmax}(z_0)$ the clean distribution (all symbols collected in Table 5). The single-unit ablation effect is $\delta z_u = z_0 - z_{\{u\}}$.

2.1 THE CONDITIONAL CO-ABLATION SCORE

A Fisher geometry over ablations. We measure ablation effects in the metric the output distribution induces (Amari, 1998). The Fisher information of the categorical output in logit coordinates, $F = \text{diag}(p_0) - p_0 p_0^\top$, is exactly the Hessian of $\text{KL}(p_0 \parallel \text{softmax}(z))$ at z_0 , so a logit perturbation δz has second-order KL cost $\frac{1}{2} \delta z^\top F \delta z + O(\|\delta z\|^3)$. We realize this metric with the centered, Fisher-weighted feature $\tilde{\delta z}_u = \sqrt{p_0} \odot (\delta z_u - \mathbb{E}_{p_0}[\delta z_u] \mathbf{1})$ on the top- r logits. Centering subtracts the shared logit-shift that an ablation imparts to every output coordinate at once, leaving only the part of the perturbation that changes the *shape* of the distribution; the $\sqrt{p_0}$ weighting then makes the plain inner product coincide with the Fisher form, $\langle \tilde{\delta z}_u, \tilde{\delta z}_v \rangle = \delta z_u^\top F \delta z_v$ (Proposition 1), so $\mathcal{E}(\delta z_u) := \mathbb{E}_{x,t} \|\tilde{\delta z}_u\|^2$ is the mean KL energy of ablating u . Collecting the centered features into a design matrix \tilde{D} (one column per unit, its rows running over the top- r logits at each of the P calibration positions) gives the Gram (hence PSD) kernel $\mathbf{H} = \frac{1}{P} \tilde{D}^\top \tilde{D}$ and the Fisher-cosine affinity $A_{uv} = \mathbf{H}_{uv} / \sqrt{\mathbf{H}_{uu} \mathbf{H}_{vv}} \in [-1, 1]$, our first-order baseline (close to recent weight-space head kernels (Yamagiwa et al., 2026)). Built from *single* ablations, \mathbf{H} is stable but first-order; the genuinely second-order content that recovers compensation lives in two objects it omits, and the rest of this section builds them.

Pairwise synergy. For units u, v , let $\delta z_{uv} = z_0 - z_{\{u,v\}}$ be the joint-ablation perturbation. The synergy is the non-additive part,

$$I_{uv} = \delta z_{uv} - \delta z_u - \delta z_v, \quad S_{uv} = \mathbb{E}_{x,t} \|\tilde{I}_{uv}\|^2, \quad (1)$$

which vanishes when units act independently and is large when u and v *compensate* for one another. It captures symmetric cooperation that first-order affinity does not model.

The COAX score. A backup is dormant until the primaries are gone, so we score units not in isolation but *after conditioning* on a seed set \mathcal{S} (typically the high-saliency primaries).

Definition 1 (Conditional co-ablation score). *The conditional ablation effect of a unit u given \mathcal{S} is its marginal effect once \mathcal{S} is already ablated, $\delta z_{u|\mathcal{S}} = z_{\mathcal{S}} - z_{\mathcal{S} \cup \{u\}}$ (so $\delta z_u \equiv \delta z_{u|\emptyset}$), with energy $\mathcal{E}(\delta z_u | \mathcal{S}) = \mathbb{E}_{x,t} \|\tilde{\delta z}_{u|\mathcal{S}}\|^2$. The COAX score is the growth of this energy under conditioning,*

$$\text{comp}_u(\mathcal{S}) = \mathcal{E}(\delta z_u | \mathcal{S}) - \mathcal{E}(\delta z_u | \emptyset). \quad (2)$$

This *conditional growth* is large for backups, whose effect appears only once \mathcal{S} is ablated, and near zero for non-redundant units. Computing it costs $O(|\mathcal{U}|)$ forward passes per seed – the same order as one single-ablation scan, and far below the $O(|\mathcal{U}|^2)$ of enumerating all pairs explicitly – so the conditional form is what lets the second-order signal scale to large models. The algorithm, its cost, and its calibration-data efficiency are in Appendix A.

Division of labor. The two signals are the two faces of non-additivity and answer two different questions. Pairwise synergy I_{uv} is the lens for *cooperation*, recovering symmetric same-circuit structure. The COAX score $\text{comp}_u(\mathcal{S})$ is the lens for *substitution*, recovering dormant backups as a node-level *compensating set*. The headline discovery and all applications use the COAX score; synergy carries the same-circuit analysis of Table 28. A glossary of the terms (primary seed, backup candidate, compensating set, conditional growth, circuit completion) is given in Appendix A.1.1.

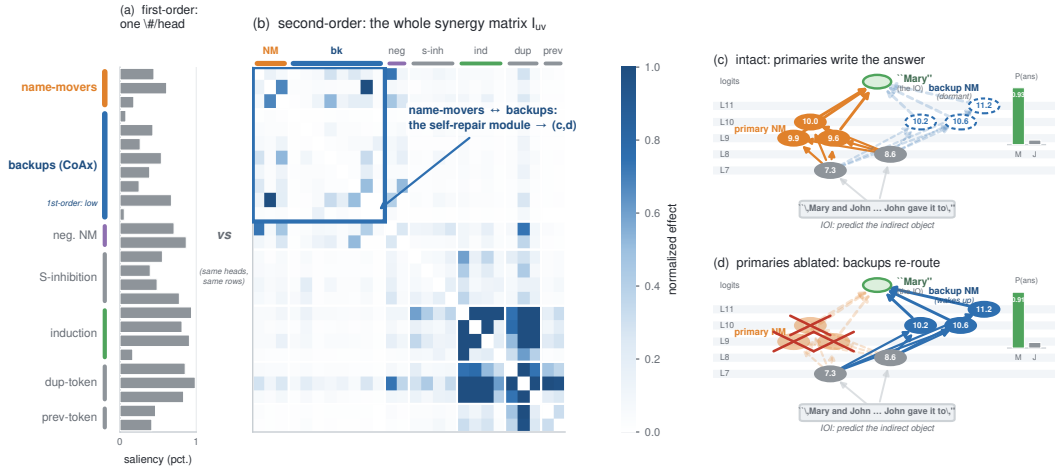


Figure 2: **The second-order structure COAX exploits, and the circuit it is** (GPT-2-small). (a) First-order scoring gives one number per head; (b) the pairwise synergy I_{uv} is a whole matrix, where the name-movers and their backups form a bright off-diagonal block (boxed), the *self-repair module* a per-head score cannot see. (c,d) The primaries write the answer while the backups stay dormant (c) while ablating the primaries wakes the backups, which re-route to the logit (d).

2.2 WHY FIRST-ORDER MISSES BACKUPS AND COAX DOES NOT

Three short results make the construction precise and explain the empirics with proofs in Appendix A.1.3. The first grounds the geometry.

Proposition 1 (Fisher identity). *For any two ablation effects, $\langle \tilde{\delta z}_u, \tilde{\delta z}_v \rangle = \delta z_u^\top F \delta z_v$ with $F = \text{diag}(p_0) - p_0 p_0^\top$. Consequently \mathbf{H} is a positive-semidefinite Fisher Gram matrix and $\mathcal{E}(\delta z_u) = \mathbb{E}_{x,t}[\delta z_u^\top F \delta z_u]$ is the mean KL energy of ablating u (twice its second-order KL cost). The centering term is exactly the $-p_0 p_0^\top$ of the Fisher form.*

The next formalizes the blind spot. Call a unit a *pure backup* for \mathcal{S} if it is dormant on the clean model ($\delta z_b = 0$, equivalently zero clean activation) yet carries the effect once \mathcal{S} is ablated ($\mathcal{E}(\delta z_b | \mathcal{S}) = \Delta > 0$); a unit is *inert* if it is silent throughout – zero clean activation, $\delta z_u = 0$, and $\mathcal{E}(\delta z_u | \mathcal{S}) = 0$.

Proposition 2 (Additivity blind spot). *Let a score assign unit u the value $g(\theta_u)$ for some fixed g and a per-unit statistic θ_u computed from the clean forward/backward pass. If θ is invariant between a pure backup and an inert unit (as any function of a unit’s clean-state marginal effect or clean activation is, since both vanish for a dormant unit), the score assigns the two the same value and cannot rank one above the other. By contrast $\text{comp}_b(\mathcal{S}) = \Delta > 0$ while $\text{comp}_{\text{inert}}(\mathcal{S}) = 0$, so COAX separates them.*

The third explains *why* the conditional score works and unifies the two signals: a dormant backup’s conditional growth is its second-order coupling to the seed.

Proposition 3 (Conditional growth is seed synergy). *Under a pairwise-interaction truncation of the joint ablation effect, $\delta z_u | \mathcal{S} = \delta z_u + \sum_{s \in \mathcal{S}} I_{su}$, hence $\text{comp}_u(\mathcal{S}) = \mathbb{E}_{x,t} [2 \langle \tilde{\delta z}_u, \sum_s \tilde{I}_{su} \rangle + \|\sum_s \tilde{I}_{su}\|^2]$. For a dormant unit ($\delta z_u \approx 0$), $\text{comp}_u(\mathcal{S}) \approx \mathbb{E}_{x,t} \|\sum_{s \in \mathcal{S}} \tilde{I}_{su}\|^2$, the energy of its synergistic coupling to the seed.*

Together, these results give the picture. A backup is an output-space *substitute* for the primaries: it writes a correlated logit direction, so its synergy I_{sb} with the seed is large even as its solo effect δz_b stays small. Proposition 2 makes such a head invisible to any score meeting its invariance condition; Proposition 3 shows that comp reads exactly the off-diagonal interaction those scores discard, so it is genuinely second-order rather than an output-grounded re-ablation. On IOI the name-movers and their backups bind into a dense high-synergy *module* (Figure 2): off-diagonal mass in I_{uv} that single-ablation saliency, reading only the diagonal, leaves dark, which is why the backups occupy the low-saliency, high-COAX corner of Figure 1a. The methods we test meet the idealized invariance only

Table 1: **Backup-head discovery** (GPT-2-small, node-level ROC-AUC over the eight documented backups, mean $_{\pm\text{std}}$, 4 seeds). Additive, gradient-based, and self-repair-aware scores fall short; COAX exposes the backups (primaries, right, are easy for all). \dagger Given COAX’s primary-ablated seed, the fair comparison is the seeded GIM (0.63), not the seed-free AtP* (0.82).

signal	backup	primary
single ablation (1st)	0.33 \pm 0.00	0.43 \pm 0.03
AtP (1st)	0.60 \pm 0.03	0.81 \pm 0.01
GIM-style \dagger (1st)	0.63 \pm 0.05	—
EAP-IG (1st)	0.70 \pm 0.02	0.75 \pm 0.03
AtP* GradDrop (1st)	0.82 \pm 0.03	—
COAX \dagger (2nd, ours)	0.91 \pm 0.00	—

Table 2: **Completion module.** Adding COAX backups to a circuit found *automatically* by each first-order finder (top-3 heads) roughly doubles the joint-ablation IOI logit-difference drop, far above random; it ties the finder’s own next- m heads (+own) while recruiting *lower*-ranked heads, so the value is *which* heads, not faithfulness (§3.4; 2 seeds, $m=4$).

finder	prim.	+COAX	+own	+rand	FO pct.
AtP	1.28	3.11	3.09	1.69	0.80
EAP-IG	0.68	1.71	1.75	0.95	0.81
AtP*	1.85	3.73	3.77	2.25	0.45

approximately, weighting each unit by clean-state statistics that nearly vanish for a near-dormant backup; this is why they land at 0.33–0.82 rather than chance, while COAX reaches 0.91 (Table 1).

3 COMPLETING CIRCUITS BY RECOVERING BACKUPS

We establish COAX on GPT-2-small IOI, the one circuit with labeled backups. In turn, we **recover** the documented backups, **verify** they are mechanistically real, check their **faithfulness, completeness, and minimality**, **complete** circuits found automatically by first-order methods, and show the discovery **generalizes** across scale and architecture.

Protocol. We use the GPT-2-small (Radford et al., 2019) IOI circuit (Wang et al., 2022), the only one with head-level backup ground truth. Two ROC-AUCs appear and are never compared: *backup-AUC* is node-level, ranking the documented backups given the primaries (the headline metric of Table 1), and *cluster-AUC* is pair-level, scoring whether two heads share a circuit (Table 28). Backup-discovery numbers are means over 4 prompt seeds (std ≤ 0.04); the controls, per-experiment seed counts, and full protocol are in Appendix B.

3.1 BACKUP DISCOVERY

Table 1 is the central result. Backup name-movers are hard for *every* node-ranking baseline we test, including those explicitly designed for self-repair: single-ablation saliency (0.33), attribution patching (0.60), a self-repair-aware GIM adaptation (0.63), and EAP-IG (0.70), a strong circuit-localization baseline on the Mechanistic Interpretability Benchmark (MIB) (Mueller et al., 2025). The strongest is AtP* with GradDrop (0.82) (Kramár et al., 2024), whose gradient-dropout is built to catch the direct-versus-indirect gradient cancellation self-repair induces; it leads the other gradient-corrected methods yet still trails COAX at 0.91. The gradient baselines locate the *primary* name-movers well (≈ 0.78 ; single ablation is itself partly masked at 0.43). The gap is not about conditioning or a smarter gradient but the *node-additive form itself*: a backup’s contribution is a non-additive substitution that no additive score, however corrected, can model. Conditioning on the primaries and reading the growth in ablation effect (Eq. 2) makes the backups visible: COAX places 6 of the 8 documented backups in its top 20 of 141 candidates (top-10 recall 4/8), far above chance.

One control deserves flagging up front: an input-side *co-activation* score also ranks the IOI backups highly (0.92 AUC), since they co-fire with the primaries, so COAX is not the only signal that finds them. But co-activation is correlational: it offers no causal or patching validation, it collapses on movement circuits (duplicate-token 0.32 vs. COAX’s 0.97), and used as a completion signal it *over*-ablates, its top- k pulling in co-firing core heads and flipping the IOI logit-difference sign (Appendix C.1.2). We therefore treat it separately (Section 5) and keep causal node-ranking scores.

COAX completes; it does not discover from scratch. COAX uses a primary seed, so we state both directions. The *fair* comparison gives a baseline the *same* seed: our GIM-style gradient on the

primary-ablated model still reaches only 0.63, so conditioning is not enough, and it is the *form* of the score (full-distribution conditional growth, not a metric gradient) that recovers the backups. Conversely, as a *standalone* finder that must detect its own seed, COAX peaks at 0.60 (Appendix C.5.1), below the seed-free AtP* (0.82). The 0.91 headline is thus a *completion* result with documented primaries as the seed, not standalone discovery.

What the IOI numbers establish. The ranking is statistically far from chance, by two tests that do not lean on the small positive set: a label-permutation test places the 0.91 AUC entirely outside the null ($p < 10^{-4}$), and a hypergeometric top- k test is significant at every cutoff (6/8 in the top 20, $p = 9 \times 10^{-5}$). The head-to-head comparison needs more care, because a backup score is only meaningful once it holds the primary seed. Against the fair, same-seed baseline – the seeded GIM at 0.63 – the 0.26 gap is significant under a paired DeLong test over the eight backups (DeLong et al., 1988) ($p = 2 \times 10^{-3}$). The smaller 0.09 gap over the seed-free AtP* (0.82) holds in every seed but is underpowered on only eight positives; that under-power is an artifact of comparing against a baseline denied the seed, not evidence the effect is fragile (all tests, and across-seed variants, in Appendix C.1.3).

Because eight documented backups cannot supply a powered head-to-head comparison, a controlled-redundancy synthetic benchmark does (Table 12, Appendix C.1.4). With 100 planted backups the clean-state scores stay at or below chance – first-order energy at 0.42 actively *anti*-ranks them – while COAX reaches 0.90 ($p < 10^{-15}$), exactly as Proposition 2 predicts. The benchmark also isolates *which* property of the score does the work, and it is not conditioning alone: a conditional but answer-aligned GIM proxy reaches 0.85 yet collapses where the real IOI backups live, off the answer direction (all eight have $\beta < 0.01$, an energy fraction rather than a causal weight). Reading the full conditional distribution, COAX stays invariant there – the same reason the real GIM reaches only 0.63 on IOI (Appendix C.1.4).

3.2 ARE THE DISCOVERED HEADS REAL BACKUPS?

A discovery method must surface heads that *behave* like backups, not merely match labels. For the top-10 heads by COAX score we measure two label-free signatures: the *activation ratio* (output norm with primaries ablated over clean) and the *conditional causal effect* (the logit-difference drop from ablating the head once the primaries are gone). The documented backups among the top-10 score 1.21 and +0.21 on these, versus 1.03 and -0.12 for the other surfaced heads; keeping only heads that both wake up and are load-bearing raises documented-backup precision in the top-10 from 0.40 to 1.00 (Appendix C). To rule out circularity, an *independent* structural check (a name-mover attends to and copies the IO token (Wang et al., 2022)) ranks the backups at 0.96 ROC-AUC while sharing none of COAX’s machinery (Spearman $\rho = 0.09$), corroborating the discovery rather than restating it (the bespoke read does not transfer to other circuits; Appendix C).

How the backups take over. Beyond labels, we trace the hand-off directly (Figure 3). As we ablate more of the primary name-movers ($k = 0, 1, 2, 3$, strongest first), the discovered backups *wake up* monotonically – their output-norm ratio climbs from 1.00 to 1.15 and their conditional causal drop from +0.05 to +0.11 – while a matched random control stays flat. A direct-logit-attribution (nostalgebraist, 2020) decomposition confirms a genuine hand-off: the primary name-movers carry large positive clean DLA to the IO – S direction (+0.76), and the backups’ DLA to the answer more than doubles once the primaries are ablated (+0.07 → +0.21). Finally, counterfactual patching (Zhang & Nanda, 2024) closes the causal loop: ablating the primaries but *freezing* the backups to their dormant value removes 55% of the self-repair, while freezing a matched random set removes none (Figure 3d). The backups’ *wake-up* causally drives the repair, not mere correlation.

3.3 FAITHFULNESS, COMPLETENESS, AND MINIMALITY

A discovered circuit is judged by three community-standard criteria (Wang et al., 2022): it should be *faithful* (reproduce the behavior), *complete* (contain every component the model uses), and *minimal* (every component is necessary). Self-repair is precisely a *completeness* failure (it is how the IOI backups were first noticed), so completeness is the criterion that most sharply separates COAX from first-order discovery, and we report all three.

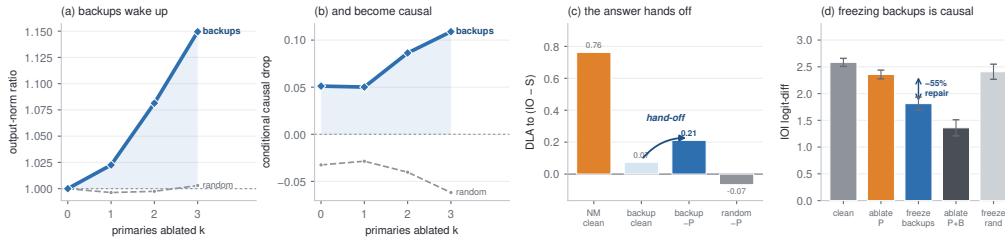


Figure 3: **How the discovered backups take over (GPT-2-small).** As primaries are ablated (k), the backups grow in output norm (a) and conditional causal effect (b) while random heads stay flat; the answer’s direct logit attribution hands off to them (c); and freezing their dormant activations removes 55% of the self-repair (d), confirming the wake-up is causal.

Completeness. A circuit is complete if it reproduces the full model’s *response* to ablating its members. We mean-ablate every head outside a circuit and measure how its IOI logit-difference responds to ablating the name-movers, relative to the full model. The first-order circuit (the documented IOI circuit *without* its backups, which is what an additive method recovers) is badly incomplete (gap 0.72): it cannot reproduce the self-repair the model performs. Completing it with the COAX backups closes the gap to 0.15, matching the complete documented circuit (0.16), whereas a matched-random completion does not (0.61). The dose-response curve of Figure 1c is the same completeness statement drawn as a trajectory.

Minimality check. The recovered set is enriched for individually necessary compensators: once the name-movers are ablated, the documented backups among the surfaced heads have positive mean conditional logit-difference drop (+0.21) while non-backup surfaced heads average negative (−0.12, §3.2). Individual-head drops are noisy (App. C), so we read this as *evidence* for minimality, not proof every selected head is necessary.

Faithfulness. Counterfactual patching (Figure 3d) gives the causal form of faithfulness: the completed circuit’s backups are the components the model actually *uses* under intervention – freezing them to their dormant state removes over half of the self-repair, while freezing random heads removes none.

3.4 COAX AS A COMPLETION MODULE

In practice the primary seed comes from a first-order method, so the realistic test is whether COAX *completes* an automatically discovered circuit. Seeding it with the top-3 heads of AtP, EAP-IG, or AtP* and adding its top-4 backups roughly doubles the joint-ablation IOI logit-difference drop, far above a matched-random control (AtP 1.28 → 3.11 vs random 1.69; EAP-IG 0.68 → 1.71 vs 0.95; AtP* 1.85 → 3.73 vs 2.25; Table 2), so COAX runs end-to-end and label-free, not only on documented seeds. Two qualifications temper this. On *raw* faithfulness it merely ties extending the circuit by the finder’s own next-4 heads (+own), though it recruits far lower-ranked ones (mean first-order percentile 0.69 vs 0.97); what makes the *identity* of the heads matter, not their number, is the knockout of §4, where +own overshoots into the core circuit (0.24) while COAX matches the documented set (0.70, Table 4). And completion quality tracks seed quality: under a noisy seed the recruited heads are mid-ranked compensators of *that* seed rather than the cleanly dormant backups recovered from documented primaries (Appendix C.4.2).

Same-circuit structure, and a built-in ablation. The same second-order signal also clusters *same-circuit* heads (cluster-AUC, full table Appendix E.6): pairwise synergy wins decisively on the information-movement circuits over both input-side controls (duplicate-token 0.97 vs. 0.32/0.59; induction 0.94 vs. 0.75/0.89), because these heads share aligned *output effects* but neither correlated activations nor aligned value subspaces, while co-activation wins the co-located writing heads – the two lenses are complementary. This doubles as an ablation of COAX: dropping the second-order term collapses name-mover clustering from 0.76 to 0.34, so the gain is the interaction term, not merely output-grounded ablation.

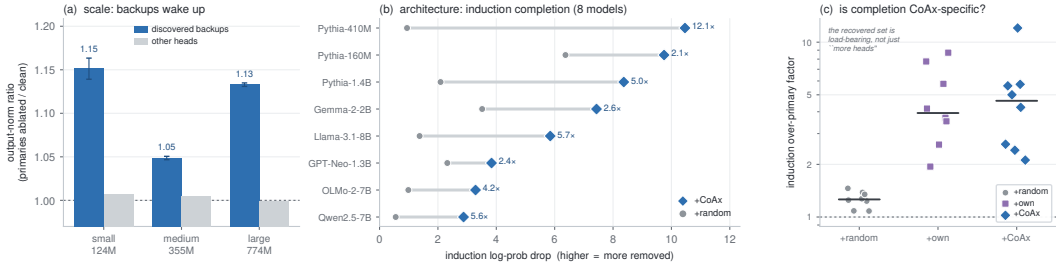


Figure 4: **The backup discovery generalizes along two axes.** (a) *Scale*: the discovered IOI backups wake up under primary ablation across the GPT-2 family (blue, above the rest of the model in grey). (b) *Architecture*: label-free induction completion on eight models from six families, where COAX drops the induction log-probability far more than matched-random. (c) A $+own$ control: both $+COAX$ and $+own$ sit far above the random floor and are comparable, as expected when induction’s redundancy is shared among homogeneous heads (§3.5).

3.5 GENERALIZATION: SCALE AND ARCHITECTURE

IOI is the only circuit with documented head-level backups, so we test that the discovery generalizes along two axes (Figure 4): *scale*, the same IOI circuit on larger models, and *architecture*, a second redundant circuit (induction) across model families.

Scale: backups replicate across the GPT-2 family. We run the identical label-free pipeline (detect the name-mover primaries by direct-logit attribution, recover compensators by conditional growth, validate by mechanism) on GPT-2 medium and large, which carry *no* backup labels. On every size the recovered set wakes up when the primaries are ablated – its output-norm ratio is 1.15, 1.05, and 1.13 (small, medium, large) versus ≈ 1.00 for the rest of the model (≤ 0.01 std over two seeds; Figure 4a) – and is load-bearing only then (Appendix C). The headline backup structure is not a GPT-2-small artifact.

Architecture: conditional completion transfers across families. We apply COAX to *induction*, a second attention-mediated circuit known to be redundant across heads (Olsson et al., 2022), with a *fully* label-free pipeline that also detects the primaries. On GPT-2-small, seeding the documented induction heads returns a compensating set that is necessary only once the primaries are gone (conditional causal drop 0.89 versus 0.05 random); ablating the primaries barely moves the induction log-probability (drop 0.27), but adding the discovered compensators drops it by 8.5, about $10\times$ the matched-random control. This holds on *eight* further models spanning *six* architecture families (Figure 4b), with attribution factors of 2.1 to $12\times$. A stronger $+own$ control (the model’s own next-strongest induction heads; Figure 4c) confirms the recovered set is load-bearing, but COAX and $+own$ are comparable here: induction’s redundancy is shared among co-firing *homogeneous* heads, with no distinct backup class to single out, so we claim label-free *recovery*, not unique identification (Appendix C).

Scope and regime. COAX targets the harder *dormant-substitution* regime, where a unit is silent until a primary is removed (IOI) and first-order scoring provably fails (Prop. 2). Where redundancy is instead shared among units that already co-fire (induction is closer to this) the components are not hidden, so even input-side co-activation finds them and COAX is complementary there, not a replacement. At the other extreme the head-level signal does not transfer to the MLP-dominated greater-than circuit (Hanna et al., 2023) (a preliminary FFN-group probe recovers only $1.5\times$ over random, within one std), suggesting greater-than carries much weaker recoverable self-repair at this granularity – a property of the circuit, not the unit (Appendix C.4.3). The recovery is robust to the primary seed, the ablation value, and the prompt template, but the seed must be the *functional* primary circuit; full seed, template, and cross-model-geometry sweeps are in the appendix.

Table 3: **Attribution recovery** (GPT-2-small IOI logit-difference drop from ablating the name-mover primaries plus a top-up set, 4 seeds; clean 2.53). The label-free COAX backups recover the masked causal effect, **exceeding** the matched-random and documented-backup top-ups.

top-up set	prim. only	+rand	+doc.	+COAX
logit-difference drop	0.22	1.0±0.7	1.15	1.76

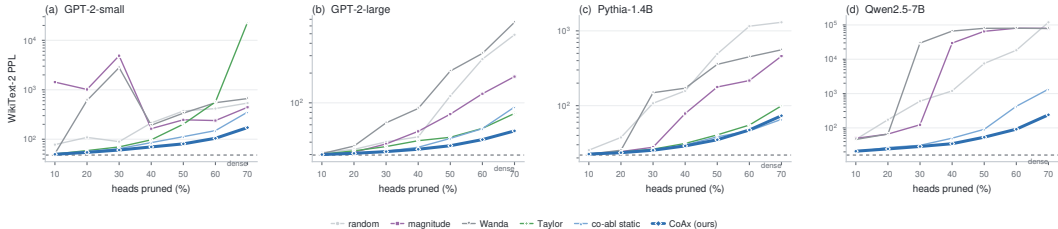


Figure 5: **Repair-aware pruning across scales** (WikiText-2 perplexity vs. heads pruned, log). **(a–d)** On four models from 124M to 7B, classical and gradient baselines degrade sharply while the self-repair-aware co-ablation order (blue) stays nearest dense at every scale; the knockout payoff of the same score is in Figure 1c. Zero-shot accuracy and the full sweep: Appendix E.

Table 4: **Capability removal** (GPT-2-small IOI accuracy under ablation, mean over 4 seeds; per-seed in Appendix D). Ablating the primary circuit leaves the behavior intact (self-repair); adding the label-free COAX backups removes it and **matches the documented oracle** (0.70 vs 0.72), whereas a first-order top-up (+own) *overshoots* to 0.24 into the core heads.

ablating set	clean	−prim.	+COAX	+own	+rand	+doc.
IOI accuracy	1.00	0.97	0.70	0.24	0.81	<u>0.72</u>

4 CLOSING THE LOOP: ATTRIBUTION, KNOCKOUT, AND PRUNING

A blind spot in component importance does not stay confined to discovery. Attribution, knockout, and pruning all rank components by the same node-additive score, so each inherits the same error wherever a circuit is redundant: it under-credits the primary whose damage is repaired and overlooks the backup that repairs it. We close the loop by feeding the recovered backups – the output of COAX, computed once and label-free – back into all three pipelines. That one set serves all three: it restores the causal effect self-repair had hidden from attribution, supplies exactly the compensators a capability knockout must also remove, and yields a pruning order that keeps a backup once its primary is gone. The paper’s thesis is in this sense operational and not merely diagnostic: conditioning on what has already been removed repairs the measurements the blind spot had distorted.

4.1 ATTRIBUTION: RECOVERING THE MASKED CAUSAL EFFECT

Attribution asks how much a set of heads is worth, read off as the behavioral change when they are ablated. On the IOI name-movers that question returns the wrong answer: ablating the primaries alone drops the logit-difference by only 0.22 (four-seed mean, clean 2.53; the single-seed value is 0.11, reconciled in Appendix D), because their backups absorb the damage. Re-attributing the same set together with the COAX backups recovers a 1.76 drop (Table 3) – the effect the redundancy had hidden. We benchmark this against the two controls that matter, rather than the inflated ratio over the over-masked baseline: it exceeds a matched random top-up (1.0±0.7) and even the curated documented backups (1.15) at every seed. The margin over the documented set is small but consistent, which we read as a hint that the hand-annotated list does not exhaust the functional compensators – the extra surfaced heads carry the same backup signature (Appendix C) – rather than as noise.

4.2 CIRCUIT KNOCKOUT: A CAPABILITY NEEDS ITS BACKUPS REMOVED

Knockout is the mirror image of attribution: to disable a behavior one must remove its backups too, or self-repair restores it. Ablating the documented name-mover primaries – the heads a first-order analysis would call “the circuit” – barely dents IOI accuracy (1.00 \rightarrow 0.97); the behavior survives, fully masked (Table 4, 4 seeds). Adding the label-free COAX backups is what brings accuracy down to 0.70, matching the documented-backup oracle (0.72). What turns this into a statement about *which* heads rather than how many is the first-order top-up: extending the ablation by the same number of the model’s own next-ranked heads overshoots to 0.24, cutting past the backups into the core name-movers (Figure 1c). COAX recovers the specific compensators a complete knockout needs, not merely more of them. Accuracy need not fall to chance – IOI retains redundancy beyond the name-mover family – so the informative quantity is the ordering across sets, not the absolute floor.

4.3 PRUNING: A REPAIR-AWARE REMOVAL ORDER

A one-shot pruner scores every head independently, so self-repair hides a redundant group’s *joint* importance: a primary and its backup each rate low on their own, the group is pruned together, and the behavior it carried collapses. The fix is again conditioning. We prune sequentially, re-measuring the COAX score after each removal, so a backup’s importance rises the moment its primary leaves and the pruner keeps it. The benefit comes in two layers (Figure 5a–d; full sweep Appendix E). First, the co-ablation energy is already a strong standalone head score: across four models from 124M to 7B it beats every weight-, magnitude-, and gradient-based baseline, including the strong gradient-Taylor order wherever Taylor is defined (50%-sparsity perplexity 80.6 vs 201.4 on GPT-2-small, with the margin holding on GPT-2-large and Pythia-1.4B). Second, re-measuring sequentially adds a further self-repair-aware gain that widens with sparsity (80.6 vs 112.6 for the static order); because the two orders share the identical signal and differ only in the conditioning, this increment isolates the value of conditioning itself. The dominant effect is the better head score, which the sequential pass then refines – the same conditional principle, now used to retain the very components a behavior depends on. Zero-shot accuracy tells the same story (Appendix E).

5 RELATED WORK

Most automated discovery relies on additive scores. ACDC (Conmy et al., 2023), attribution and edge patching (Syed et al., 2023), EAP-IG (Hanna et al., 2024), and AtP* (Kramár et al., 2024) score a component by its single-node effect and select greedily; Conmy et al. (2023) already observe that this systematically misses the negative and compensating components a circuit relies on. A newer wave (sparse feature circuits (Marks et al., 2024), information-flow routes (Ferrando & Voita, 2024), contextual decomposition (Hsu et al., 2025), and edge pruning (Bhaskar et al., 2024)) refines the search but still selects through additive or locally linear scores, and so inherits the same blind spot. Our pairwise synergy I_{uv} is the second-order correction these methods omit: COAX beats EAP-IG (strong on MIB (Mueller et al., 2025)) and AtP* on backup recovery while matching them on the non-redundant primaries, so it adds the missing axis without giving up the one they already have.

Self-repair and redundancy. The Hydra effect (McGrath et al., 2023), IOI backup name-movers (Wang et al., 2022), copy-suppression (McDougall et al., 2023), and anti-erasure mechanisms (Rushing & Nanda, 2024) are established by manual knock-out-and-inspect. Methods that *automate* around self-repair either *diagnose* it (Ye (2026) show joint ablation does up to an order of magnitude more damage than summed single ablations) or *de-bias a node’s own score* to undo the masking (GIM (Edin et al., 2025); AtP* GradDrop (Kramár et al., 2024)). Both keep importance node-additive, so neither names the compensating heads; COAX does, and confirms them causally. A fair GIM that shares our seed still reaches only 0.63 versus 0.91, which pins the gap to the node-additive *form* rather than to conditioning.

Second-order and interaction-aware importance. Second-order structure underlies weight pruning, from Optimal Brain Damage (LeCun et al., 1989) to the Fisher framework of Kwon et al. (2022); inference-time pruners select pathways from representation–parameter probes (Gong et al.,

2026), an input-side signal complementary to our output-grounded order. Neuron Shapley (Ghorbani & Zou, 2020) accounts for interactions but by combinatorial sampling, not a closed-form output-grounded kernel. Closest in vocabulary is the concurrent synergistic core (Urbina-Rodriguez et al., 2026), which ranks heads by the information-theoretic synergy of their *activation* statistics, an input-side and correlational notion. This input-side family is strong on IOI, where the backups co-fire with the name-movers (co-activation alone reaches 0.92 AUC), so we do not claim COAX is the only signal that finds them. But being correlational it gives no causal or patching validation, collapses on movement circuits, and over-ablates when used to complete a circuit (§3.1, Appendix C.1.2). COAX is the opposite kind of measurement – causal and output-grounded – which is precisely what lets it carry the downstream attribution, knockout, and pruning results that a correlational ranking cannot.

6 CONCLUSION

Self-repair shows that a component’s importance is not a property it carries alone, but one that surfaces only in relation to the rest of the circuit: the heads that matter most are often those that do nothing until another fails. Once we stop scoring units in isolation and instead ask how each responds when the primary set is removed, the redundancy that hides from first-order analysis becomes something we can name, rank, and intervene on. COAX makes that shift concrete and cheap, turning a known or discovered primary circuit into the explicit backup set behind it, and with it repairing the attribution, knockout, and pruning pipelines the blind spot had quietly corrupted. Faithful interpretability of a robust model, we argue, must therefore be *conditional*: redundancy is not noise to be averaged out but structure to be conditioned on.

REFERENCES

- Shun-Ichi Amari. Natural gradient works efficiently in learning. *Neural Computation*, 10(2):251–276, 1998.
- Leonard Bereska and Efstratios Gavves. Mechanistic interpretability for AI safety: A review. *Transactions on Machine Learning Research (TMLR)*, 2024. arXiv:2404.14082.
- Adithya Bhaskar, Alexander Wettig, Dan Friedman, and Danqi Chen. Finding transformer circuits with edge pruning. In *Advances in Neural Information Processing Systems (NeurIPS)*, 2024. arXiv:2406.16778.
- Stella Biderman, Hailey Schoelkopf, Quentin Anthony, Herbie Bradley, et al. Pythia: A suite for analyzing large language models across training and scaling. In *International Conference on Machine Learning (ICML)*, 2023.
- Yonatan Bisk, Rowan Zellers, Ronan Le Bras, Jianfeng Gao, and Yejin Choi. PIQA: Reasoning about physical commonsense in natural language. In *AAAI Conference on Artificial Intelligence*, 2020.
- Sid Black, Leo Gao, Phil Wang, Connor Leahy, and Stella Biderman. GPT-Neo: Large scale autoregressive language modeling with mesh-tensorflow. Zenodo, 2021.
- Peter Clark, Isaac Cowhey, Oren Etzioni, Tushar Khot, Ashish Sabharwal, Carissa Schoenick, and Oyvind Tafjord. Think you have solved question answering? try ARC, the AI2 reasoning challenge. arXiv:1803.05457, 2018.
- Arthur Conmy, Augustine N. Mavor-Parker, Aengus Lynch, Stefan Heimersheim, and Adrià Garriga-Alonso. Towards automated circuit discovery for mechanistic interpretability. In *Advances in Neural Information Processing Systems (NeurIPS)*, 2023. arXiv:2304.14997.
- Elizabeth R. DeLong, David M. DeLong, and Daniel L. Clarke-Pearson. Comparing the areas under two or more correlated receiver operating characteristic curves: A nonparametric approach. *Biometrics*, 44(3):837–845, 1988.
- Joakim Edin, Róbert Csordás, Tuukka Ruotsalo, Zhengxuan Wu, Maria Maistro, Casper L. Christensen, Jing Huang, and Lars Maaløe. Correcting gradient-based circuit localization via interaction-aware backpropagation (GIM), 2025.
- Nelson Elhage, Neel Nanda, Catherine Olsson, Tom Henighan, Nicholas Joseph, Ben Mann, Amanda Askell, Yuntao Bai, Anna Chen, Tom Conerly, Nova DasSarma, Dawn Drain, Deep Ganguli, Zac Hatfield-Dodds, Danny Hernandez, Andy Jones, Jackson Kernion, Liane Lovitt, Kamal Ndousse, Dario Amodei, Tom Brown, Jack Clark, Jared Kaplan, Sam McCandlish, and Chris Olah. A mathematical framework for transformer circuits, 2021. <https://transformer-circuits.pub/2021/framework/index.html>.
- Javier Ferrando and Elena Voita. Information flow routes: Automatically interpreting language models at scale, 2024.
- Gemma Team. Gemma 2: Improving open language models at a practical size. arXiv:2408.00118, 2024.
- Amirata Ghorbani and James Zou. Neuron shapley: Discovering the responsible neurons. In *Advances in Neural Information Processing Systems (NeurIPS)*, 2020. arXiv:2002.09815.
- Zhiren Gong, Yikun Hou, Fan Wu, Che Wang, Fuyao Zhang, Tiantong Wu, Yurong Hao, Jiaming Zhang, Yiyang Duan, Tiantong Wang, Fei Huang, Chau Yuen, and Wei Yang Bryan Lim. Subspacepath pruner: Inference-time pruning via probe-based representation-parameter coupling. In *International Conference on Machine Learning (ICML)*, 2026. URL <https://openreview.net/forum?id=fvkCjFvWKF>.
- Michael Hanna, Ollie Liu, and Alexandre Variengien. How does GPT-2 compute greater-than?: Interpreting mathematical abilities in a pre-trained language model. In *Advances in Neural Information Processing Systems (NeurIPS)*, 2023. arXiv:2305.00586.

- Michael Hanna, Sandro Pezzelle, and Yonatan Belinkov. Have faith in faithfulness: Going beyond circuit overlap when finding model mechanisms. In *Conference on Language Modeling (COLM)*, 2024. arXiv:2403.17806.
- Aliyah R. Hsu, Georgia Zhou, Yeshwanth Cherapanamjeri, Yaxuan Huang, Anobel Y. Odisho, Peter R. Carroll, and Bin Yu. Efficient automated circuit discovery in transformers using contextual decomposition. In *International Conference on Learning Representations (ICLR)*, 2025. arXiv:2407.00886.
- János Kramár, Tom Lieberum, Rohin Shah, and Neel Nanda. AtP*: An efficient and scalable method for localizing LLM behaviour to components, 2024.
- Woosuk Kwon, Sehoon Kim, Michael W. Mahoney, Joseph Hassoun, Kurt Keutzer, and Amir Ghomami. A fast post-training pruning framework for transformers. In *Advances in Neural Information Processing Systems (NeurIPS)*, 2022. arXiv:2204.09656.
- Yann LeCun, John S. Denker, and Sara A. Solla. Optimal brain damage. *Advances in Neural Information Processing Systems (NeurIPS)*, 1989.
- Llama Team. The llama 3 herd of models. arXiv:2407.21783, 2024.
- Samuel Marks, Can Rager, Eric J. Michaud, Yonatan Belinkov, David Bau, and Aaron Mueller. Sparse feature circuits: Discovering and editing interpretable causal graphs in language models, 2024.
- Callum McDougall, Arthur Conmy, Cody Rushing, Thomas McGrath, and Neel Nanda. Copy suppression: Comprehensively understanding an attention head, 2023.
- Thomas McGrath, Matthew Rahtz, János Kramár, Vladimir Mikulik, and Shane Legg. The hydra effect: Emergent self-repair in language model computations, 2023.
- Stephen Merity, Caiming Xiong, James Bradbury, and Richard Socher. Pointer sentinel mixture models. In *International Conference on Learning Representations (ICLR)*, 2017.
- Joseph Miller, Bilal Chughtai, and William Saunders. Transformer circuit faithfulness metrics are not robust. In *Conference on Language Modeling (COLM)*, 2024. arXiv:2407.08734.
- Pavlo Molchanov, Arun Mallya, Stephen Tyree, Iuri Frosio, and Jan Kautz. Importance estimation for neural network pruning. In *IEEE/CVF Conference on Computer Vision and Pattern Recognition (CVPR)*, 2019. arXiv:1906.10771.
- Aaron Mueller, Atticus Geiger, Sarah Wiegreffe, et al. MIB: A mechanistic interpretability benchmark, 2025. ICML 2025.
- nostalgebraist. Interpreting GPT: The logit lens. LessWrong, 2020. <https://www.lesswrong.com/posts/AcKRB8wDpdaN6v6ru/interpreting-gpt-the-logit-lens>.
- Chris Olah, Nick Cammarata, Ludwig Schubert, Gabriel Goh, Michael Petrov, and Shan Carter. Zoom in: An introduction to circuits. *Distill*, 2020. doi: 10.23915/distill.00024.001.
- OLMo Team. 2 OLMo 2 furious. arXiv:2501.00656, 2024.
- Catherine Olsson, Nelson Elhage, Neel Nanda, Nicholas Joseph, Nova DasSarma, Tom Henighan, Ben Mann, Amanda Askell, Yuntao Bai, Anna Chen, Tom Conerly, Dawn Drain, Deep Ganguli, Zac Hatfield-Dodds, Danny Hernandez, Scott Johnston, Andy Jones, Jackson Kernion, Liane Lovitt, Kamal Ndousse, Dario Amodei, Tom Brown, Jack Clark, Jared Kaplan, Sam McCandlish, and Chris Olah. In-context learning and induction heads, 2022. Transformer Circuits Thread.
- Qwen Team. Qwen2.5 technical report. arXiv:2412.15115, 2024.
- Alec Radford, Jeffrey Wu, Rewon Child, David Luan, Dario Amodei, and Ilya Sutskever. Language models are unsupervised multitask learners. *OpenAI technical report*, 2019.

- Cody Rushing and Neel Nanda. Explorations of self-repair in language models. In *International Conference on Machine Learning (ICML)*, 2024. arXiv:2402.15390.
- Mingjie Sun, Zhuang Liu, Anna Bair, and J. Zico Kolter. A simple and effective pruning approach for large language models, 2023.
- Mukund Sundararajan, Ankur Taly, and Qiqi Yan. Axiomatic attribution for deep networks. In *International Conference on Machine Learning (ICML)*, 2017. arXiv:1703.01365.
- Aaquib Syed, Can Rager, and Arthur Conmy. Attribution patching outperforms automated circuit discovery, 2023.
- Pedro Urbina-Rodriguez, Zafeirios Fountas, Fernando E. Rosas, Jun Wang, Andrea I. Luppi, Haitham Bou-Ammar, Murray Shanahan, and Pedro A. M. Mediano. A brain-like synergistic core in LLMs drives behaviour and learning, 2026.
- Kevin Wang, Alexandre Variengien, Arthur Conmy, Buck Shlegeris, and Jacob Steinhardt. Interpretability in the wild: a circuit for indirect object identification in GPT-2 small, 2022.
- Hiroaki Yamagiwa, Yusuke Takase, and Hidetoshi Shimodaira. Measuring affinity between attention-head weight subspaces via the projection kernel, 2026.
- Donald Ye. Hidden heroes and gradient bloats: Layer-wise redundancy inverts attribution in transformers, 2026.
- Rowan Zellers, Ari Holtzman, Yonatan Bisk, Ali Farhadi, and Yejin Choi. HellaSwag: Can a machine really finish your sentence? In *Annual Meeting of the Association for Computational Linguistics (ACL)*, 2019.
- Fred Zhang and Neel Nanda. Towards best practices of activation patching in language models: Metrics and methods. In *International Conference on Learning Representations (ICLR)*, 2024.

APPENDIX OVERVIEW

This appendix provides the material supporting the main text: the method details and proofs, the full experimental protocol, and the complete per-model and per-seed results behind every reported number. It is organized by topic, in the order the main text introduces them.

- **Appendix A, Method details.** In three parts: the definitions, Fisher geometry, and proofs; the algorithm, its cost, efficiency, and implementation; and the hyperparameters with the ablation-value and calibration-efficiency robustness studies.
- **Appendix B, Experimental setup.** Models, calibration and evaluation data, circuit ground truth, metric definitions, and the full baseline roster with implementation notes.
- **Appendix C, Discovery, full results.** In five parts: (i) statistical significance and controls (per-seed AUC, permutation / hypergeometric / DeLong tests, the synthetic benchmark, and the co-activation control); (ii) evidence the surfaced heads are genuine backups (wake-up and hand-off, the signature filter, a single-head case study, and circuit visualizations); (iii) what the score keys on (the feature ablation and the module’s non-additivity); (iv) generalization, completion, and scope (induction across scales and architectures, completing automatically-discovered circuits, and the greater-than boundary); and (v) robustness (primary seed and prompt template).
- **Appendix D, Attribution and removal, full results.** Per-seed attribution correction, the relation to behavior-faithfulness metrics, and the per-seed capability-removal accuracy.
- **Appendix E, Pruning and cross-scale geometry, full results.** All sparsities, models, and tasks; the Taylor baseline; per-seed downstream accuracy; the module-partition negative; and the per-model VS-ACTIVE geometry numbers for all twelve models.
- **Appendix F, Limitations, broader impact, and reproducibility.** An honest account of scope, societal impact, and the code map, commands, and compute for reproduction.

A METHOD DETAILS

A.1 DEFINITIONS, GEOMETRY, AND PROOFS

A.1.1 TERMINOLOGY

We fix the vocabulary used throughout. **Primary seed \mathcal{S}** : the components whose removal triggers compensation, supplied by the analyst or by a first-order discovery method. **Backup candidate u** : a unit whose conditional ablation effect increases after \mathcal{S} is removed. **Compensating set \mathcal{B}** : the top-ranked backup candidates COAX returns, optionally filtered by the mechanistic signatures. **Conditional growth**: the increase in Fisher ablation energy of a unit once \mathcal{S} is ablated, i.e. the COAX score $\text{comp}_u(\mathcal{S})$. **Pairwise synergy I_{uv}** : the symmetric non-additivity of jointly ablating two units. **Circuit completion**: adding a compensating set to a first-order-discovered primary circuit. We say “second-order” in the intervention sense (removing a set \neq summing its members), and reserve “backup/compensator” for candidates that also pass a behavioral sign or signature check.

Notation. Table 5 collects every symbol used in the method and proofs.

A.1.2 FISHER-WEIGHTED CO-ABLATION FEATURES

For a frozen model with dense next-token distribution p_0 at a calibration position, ablating unit u changes the logits to $z_{\{u\}}$, giving $\delta z_u = z_0 - z_{\{u\}}$. The Fisher information of the categorical output, $F = \text{diag}(p_0) - p_0 p_0^\top$, is the local second-order form of $\text{KL}(p_0 \| p_{\{u\}})$, so $\frac{1}{2} \delta z_u^\top F \delta z_u$ is, to second order, the KL cost of the ablation. We work with the centered, Fisher-weighted feature $\tilde{\delta z}_u = \sqrt{p_0} \odot (\delta z_u - \mathbb{E}_{p_0}[\delta z_u] \mathbf{1})$ on the top- r logits ($r=192$), making $\langle \tilde{\delta z}_u, \tilde{\delta z}_v \rangle$ a Fisher inner product and the Gram matrix \mathbf{H} positive semidefinite. The centering removes the shared logit-shift direction that otherwise inflates every pairwise affinity; the design ablation in Appendix C shows it is the load-bearing ingredient.

Table 5: Notation used throughout the paper.

symbol	meaning
u, v	structured units (attention heads in the main experiments)
\mathcal{U}	the set of all candidate units
\mathcal{S}	primary seed set conditioned on (Def. 1)
M	an ablated set of units; z_M the logits with M ablated
$z_0 \equiv z_\emptyset$	clean logits; $p_0 = \text{softmax}(z_0)$ the clean distribution
$\delta z_u = z_0 - z_{\{u\}}$	single-unit ablation effect (logit perturbation)
$\delta z_{u \mathcal{S}} = z_{\mathcal{S}} - z_{\mathcal{S} \cup \{u\}}$	conditional ablation effect given \mathcal{S}
$\delta z_{uv} = z_0 - z_{\{u,v\}}$	joint (pair) ablation effect
$F = \text{diag}(p_0) - p_0 p_0^\top$	Fisher information of the output (Hessian of KL at z_0)
$\tilde{\delta z}_u = \sqrt{p_0} \odot (\delta z_u - \mathbb{E}_{p_0}[\delta z_u] \mathbf{1})$	centered Fisher-weighted feature (top- r logits)
$\mathbf{H} = \frac{1}{P} \tilde{D}^\top \tilde{D}$	Fisher Gram (co-ablation curvature) kernel; PSD
$A_{uv} = \mathbf{H}_{uv} / \sqrt{\mathbf{H}_{uu} \mathbf{H}_{vv}}$	Fisher-cosine affinity $\in [-1, 1]$ (first-order baseline)
$\mathcal{E}(\delta z_u \mathcal{S}) = \mathbb{E}_{x,t} \ \delta z_{u \mathcal{S}}\ ^2$	mean KL energy of ablating u given \mathcal{S}
$\text{comp}_u(\mathcal{S}) = \mathcal{E}(\delta z_u \mathcal{S}) - \mathcal{E}(\delta z_u)$	COAX conditional-growth score (Eq. 2)
$I_{uv} = \delta z_{uv} - \delta z_u - \delta z_v$	pairwise synergy (non-additive part); $S_{uv} = \mathbb{E} \ \tilde{I}_{uv}\ ^2$
r, P	top- r logit truncation ($r=192$); number of calibration positions

A.1.3 PROOFS

Throughout, a position contributes a clean logit vector z_0 with $p_0 = \text{softmax}(z_0)$, and $\bar{a} := \mathbb{E}_{p_0}[a] = \sum_i (p_0)_i a_i$ for a vector a . The feature map $a \mapsto \tilde{a} = \sqrt{p_0} \odot (a - \bar{a} \mathbf{1})$ is linear in a .

Proof of Proposition 1. For two effects $\delta z_u, \delta z_v$,

$$\langle \tilde{\delta z}_u, \tilde{\delta z}_v \rangle = \sum_i (p_0)_i (\delta z_{u,i} - \bar{\delta z}_u) (\delta z_{v,i} - \bar{\delta z}_v) = \sum_i (p_0)_i \delta z_{u,i} \delta z_{v,i} - \bar{\delta z}_u \bar{\delta z}_v,$$

using $\sum_i (p_0)_i = 1$ and $\sum_i (p_0)_i \delta z_{u,i} = \bar{\delta z}_u$. On the other hand $\delta z_u^\top F \delta z_v = \delta z_u^\top (\text{diag}(p_0) - p_0 p_0^\top) \delta z_v = \sum_i (p_0)_i \delta z_{u,i} \delta z_{v,i} - \bar{\delta z}_u \bar{\delta z}_v$, so the two are equal. Thus $\mathbf{H} = \frac{1}{P} \tilde{D}^\top \tilde{D}$ is a Gram matrix in this inner product and is positive semidefinite, and $\mathcal{E}(\delta z_u) = \mathbb{E}_{x,t} \langle \tilde{\delta z}_u, \tilde{\delta z}_u \rangle = \mathbb{E}_{x,t} [\delta z_u^\top F \delta z_u]$. Finally F is the Hessian of $z \mapsto \text{KL}(p_0 \| \text{softmax}(z))$ at $z = z_0$ (the standard softmax Fisher), so a second-order Taylor expansion gives $\text{KL}(p_0 \| \text{softmax}(z_0 - \delta z_u)) = \frac{1}{2} \delta z_u^\top F \delta z_u + O(\|\delta z_u\|^3)$. \square

Proof of Proposition 2. Let $s(u) = g(\theta_u)$ with θ_u a per-unit statistic of the clean forward/backward pass, and suppose θ is invariant between a pure backup and an inert unit. A pure backup b has $\delta z_b = 0$ by definition and zero clean activation (it is dormant); an inert unit has the same. Hence $\theta_b = \theta_{\text{inert}}$ and $s(b) = g(\theta_b) = g(\theta_{\text{inert}}) = s(\text{inert})$, so no such score ranks b above an inert unit. By contrast $\text{comp}_b(\mathcal{S}) = \mathcal{E}(\delta z_b | \mathcal{S}) - \mathcal{E}(\delta z_b | \emptyset) = \Delta - 0 = \Delta > 0$ while $\text{comp}_{\text{inert}}(\mathcal{S}) = 0$, so COAX strictly separates them.

Which methods satisfy the hypothesis, and how tightly. Single-ablation saliency uses $\theta_u = \delta z_u$, exactly invariant for a pure backup. Gradient attributions (AtP, EAP-IG) and AtP* weight a unit by clean activations and (clean or GradDrop-perturbed) gradients evaluated at the clean state; for a perfectly dormant backup these are zero, matching an inert unit. The condition is therefore an idealization: real backups are only near-dormant (clean activation ratio ≈ 1.0), so these methods reach non-chance but sub-COAX AUC (Table 1) rather than exactly chance. We do not claim the condition holds for weight-magnitude scores, which can rank a dormant but large-weight unit highly; empirically magnitude/Wanda are nonetheless poor backup scores. \square

Proof of Proposition 3. For a set M , expand the joint ablation effect into single and interaction terms, $\delta z_M = \sum_{u \in M} \delta z_u + \sum_{\{u,v\} \subseteq M} I_{uv} + R_M$, where R_M collects interactions of order ≥ 3 (this is the Möbius expansion of the set function $M \mapsto \delta z_M$, and $I_{uv} = \delta z_{uv} - \delta z_u - \delta z_v$ recovers

the definition for $|M| = 2$). The pairwise truncation sets $R_M = 0$. Since $z_M = z_0 - \delta z_M$, the conditional effect is

$$\delta z_{u|\mathcal{S}} = z_{\mathcal{S}} - z_{\mathcal{S} \cup \{u\}} = \delta z_{\mathcal{S} \cup \{u\}} - \delta z_{\mathcal{S}} = \delta z_u + \sum_{s \in \mathcal{S}} I_{su},$$

because the terms of $\delta z_{\mathcal{S} \cup \{u\}}$ not already in $\delta z_{\mathcal{S}}$ are exactly δz_u and the pairs $\{s, u\}$ for $s \in \mathcal{S}$. Applying the linear feature map, $\tilde{\delta z}_{u|\mathcal{S}} = \tilde{\delta z}_u + \sum_s \tilde{I}_{su}$, so

$$\text{comp}_u(\mathcal{S}) = \mathbb{E}_{x,t} \left[\|\tilde{\delta z}_u + \sum_s \tilde{I}_{su}\|^2 - \|\tilde{\delta z}_u\|^2 \right] = \mathbb{E}_{x,t} \left[2\langle \tilde{\delta z}_u, \sum_s \tilde{I}_{su} \rangle + \|\sum_s \tilde{I}_{su}\|^2 \right].$$

If u is dormant, $\delta z_u \approx 0 \Rightarrow \tilde{\delta z}_u \approx 0$ and the cross term vanishes, leaving $\text{comp}_u(\mathcal{S}) \approx \mathbb{E}_{x,t} \|\sum_{s \in \mathcal{S}} \tilde{I}_{su}\|^2 \geq 0$. \square

A.2 ALGORITHM, COST, AND IMPLEMENTATION

A.2.1 ALGORITHM AND COMPLEXITY

Algorithm 1 COAX backup discovery

- 1: **Input:** frozen model, calibration set \mathcal{X} , primary seed \mathcal{S} , units \mathcal{U}
 - 2: compute dense top- r logits $z_0(x, t)$ for all positions
 - 3: $b_0[u] \leftarrow \mathcal{E}(\delta z_u | \emptyset)$ for all u {single-ablation baseline}
 - 4: ablate \mathcal{S} ; recompute logits $z_{\mathcal{S}}$
 - 5: **for** $u \in \mathcal{U} \setminus \mathcal{S}$ **do**
 - 6: ablate $\mathcal{S} \cup \{u\}$; $e_u \leftarrow \mathcal{E}(\delta z_u | \mathcal{S})$
 - 7: $\text{comp}_u(\mathcal{S}) \leftarrow e_u - b_0[u]$
 - 8: **end for**
 - 9: **return** units ranked by $\text{comp}_u(\mathcal{S})$
-

The single-unit features and one conditional pass are each $O(|\mathcal{U}|)$ forward passes. The explicit pairwise synergy is $O(|\mathcal{U}|^2)$ and is restricted to a candidate set for large models. The greedy self-repair-aware pruning order of Appendix E amortizes the same forwards: at each step it re-uses the conditional baseline and evaluates the marginal energy of every remaining unit (Algorithm 2).

Algorithm 2 Self-repair-aware sequential head pruning

- 1: **Input:** frozen model, calibration set \mathcal{X} , units \mathcal{U} , budget B
 - 2: $\mathcal{P} \leftarrow \emptyset$ {pruned set; conditioning on what is already removed}
 - 3: **while** $|\mathcal{P}| < B$ **do**
 - 4: **for** $u \in \mathcal{U} \setminus \mathcal{P}$ **do**
 - 5: $s[u] \leftarrow \mathcal{E}(\delta z_u | \mathcal{P})$ {conditional ablation energy given the pruned set}
 - 6: **end for**
 - 7: $u^* \leftarrow \arg \min_u s[u]$ {least load-bearing given what is gone}
 - 8: $\mathcal{P} \leftarrow \mathcal{P} \cup \{u^*\}$
 - 9: **end while**
 - 10: **return** prune \mathcal{P} , keep $\mathcal{U} \setminus \mathcal{P}$
-

The *static* co-ablation order scores once with $\mathcal{E}(\delta z_u | \emptyset)$ (the diagonal of \mathbf{H}) and never re-measures; the two orders share the identical signal and differ only in the conditioning on \mathcal{P} , which is what isolates the self-repair-aware gain in Appendix E.

A.2.2 COST

COAX adds a single conditional pass to the single-ablation pass, both $O(|\mathcal{U}|)$ forward passes and no backward passes. Table 6 reports the resulting wall-clock time and peak memory on one GPU: from a few seconds on GPT-2-small to about two minutes on a 1.3B model, with memory dominated by the frozen model itself.

Table 6: Cost of COAX on one GPU with 48 calibration prompts: single-unit pass and one conditional pass, both $O(|\mathcal{U}|)$ forwards; seconds and peak memory.

model	units	single	cond.	GB
GPT-2-small	144	2.9	5.7	0.8
GPT-2-medium	384	19	39	1.7
Pythia-410m	384	18	37	1.9
Gemma-2-2b	208	18	35	6.0
GPT-Neo-1.3b	384	64	128	5.6

A.2.3 EFFICIENCY

We do not claim COAX is the cheapest score – a single gradient pass costs less – but its efficiency profile is favorable in the dimensions that matter for a discovery primitive (Figure 6). **(i) Forward-only and label-free.** COAX needs no backward pass and no task gradient: it is $2|\mathcal{U}|+1$ forward passes per seed ($|\mathcal{U}|$ for the single-ablation baseline, $|\mathcal{U}|$ for the conditional pass, one for the seed-ablated reference), so it parallelizes trivially and never differentiates the model. The gradient baselines (AtP, EAP-IG, AtP*) each need a backward pass and a task metric, yet top out at 0.82. **(ii) The conditional form avoids a quadratic cost.** The second-order signal is, in its explicit form, the pairwise synergy I_{uv} over all pairs – $O(|\mathcal{U}|^2)$ forward passes ($\approx 10^4$ for GPT-2-small). The conditional score $\text{comp}_u(\mathcal{S})$ recovers the same backup-revealing information at $O(|\mathcal{U}|)$ by conditioning on the seed once rather than enumerating pairs, a $\sim 36\times$ saving at this scale that grows with model size. **(iii) Data-cheap.** Because the score is calibration-only, it is also cheap in *data*: 32 unlabeled prompts already reach 0.90 backup AUC (Figure 7a). Wall-clock and memory for the two passes are in Table 6; on GPT-2-small the full discovery is a few seconds on one GPU.

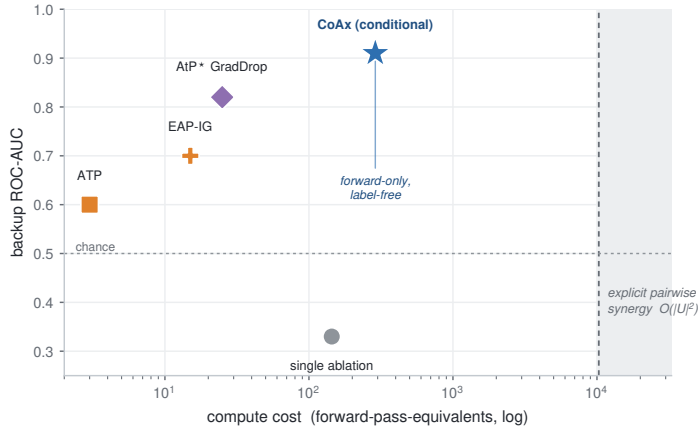


Figure 6: **Backup-recovery quality vs. compute cost** (forward-pass-equivalents; one backward = two forwards; GPT-2-small, $|\mathcal{U}|=144$, $L=12$). COAX is the only score that reaches 0.91, is forward-only and label-free, and – crucially – its conditional formulation recovers the second-order backup signal at $O(|\mathcal{U}|)$, far to the left of the $O(|\mathcal{U}|^2)$ wall of the explicit pairwise synergy it replaces. Gradient baselines are cheaper per call but require a backward pass and a task gradient and do not exceed 0.82.

Table 7 gives the per-method cost breakdown behind Figure 6: forward and backward passes (symbolically and for GPT-2-small, $|\mathcal{U}|=144$, $L=12$), forward-pass-equivalents (FPE; one backward = two forwards), whether the score is label-free, and its backup AUC. The pattern is that COAX buys the only 0.91 with forward passes alone and no labels, and its conditional route is $\sim 36\times$ cheaper than the explicit pairwise synergy that carries the same second-order signal.

[†]The explicit pairwise route carries the same second-order signal as the conditional COAX score (Proposition 3) but enumerates all pairs; COAX recovers it at $O(|\mathcal{U}|)$ by conditioning on the seed once, which is the efficiency point.

Table 7: Compute cost per backup-scoring method (GPT-2-small). FPE = forwards +2× backwards. COAX is forward-only and label-free; its conditional formulation avoids the $O(|\mathcal{U}|^2)$ explicit pairwise route while reaching the highest AUC.

method	forwards	backwards	FPE	label-free	backup AUC
single ablation (1st)	$ \mathcal{U} $	0	144	✓	0.33
ATP (1st)	1	1	3	—	0.60
EAP-IG (1st)	5	5	15	—	0.70
ATP* GradDrop (1st)	1	L	25	—	0.82
explicit pairwise synergy (2nd)	$ \mathcal{U} ^2/2$	0	$\sim 10^4$	✓	— [†]
COAX conditional (2nd, ours)	$2 \mathcal{U} +1$	0	289	✓	0.91

A.2.4 IMPLEMENTATION DETAILS

We make the score precise to support reproduction.

- **Energy.** $\mathcal{E}(\delta z_u | \mathcal{S}) = \mathbb{E}_{x,t} \|\tilde{\delta z_{u|\mathcal{S}}}\|^2$ is the mean squared Fisher norm of the conditional perturbation, averaged first over token positions within a prompt and then over prompts (equal weight per prompt).
- **Top- r logits.** The top- r index set is taken once from the *clean* distribution p_0 and held fixed across all ablated passes, so features live in a common space.
- **Seed ablation.** The primary set \mathcal{S} is ablated *jointly* (all its heads zeroed together), not seeded one at a time, and the conditional baseline $z_{\mathcal{S}}$ is shared across all units to make the pass $O(|\mathcal{U}|)$.
- **Self-exclusion.** The score is computed only for $u \notin \mathcal{S}$.
- **Ranking.** We rank by $\text{comp}_u(\mathcal{S})$ directly; no ReLU or thresholding. Negative values (units that *lose* effect once \mathcal{S} is gone) simply rank low.
- **GQA units.** Under grouped-query attention, a unit is a KV-aligned query group, so ablation respects the shared key-value head.

A.3 HYPERPARAMETERS AND ROBUSTNESS

A.3.1 HYPERPARAMETERS

Top- r logits $r=192$ (backup AUC stable within 0.01 for $r \in \{96, 192, 384\}$); 96 IOI-exercised prompts for discovery; 48 to 64 calibration windows for pruning. Zero ablation by default. Pruning interaction strength $\lambda=1.0$, reduced to about 0.5 for GQA models where FFN units over-correlate. Primary set size is the documented primary count (three name-movers for IOI, four induction heads); results are stable for seed sizes 2 to 3 (Appendix C.5.1). Table 8 consolidates every hyperparameter and random seed.

Table 8: All COAX hyperparameters and protocol constants, consolidated. Values are shared across experiments unless a section states otherwise.

knob	value
top- r logits	192 (stable for $r \in \{96, 192, 384\}$)
discovery prompts	96 IOI-exercised
calibration windows (pruning)	48–64
ablation value	zero (default; variants in Tab. 9)
interaction strength λ	1.0 (0.5 for GQA models)
primary seed $ \mathcal{S} $	documented count (3 name-movers, 4 induction)
FFN-group size	96 groups (GPT-2-small)
EAP-IG integration steps	5
prompt seeds	{42, 1, 8, 22}
random-control draws	20 (attribution / knockout)
permutation shuffles	10,000
synthetic trials	40

A.3.2 ROBUSTNESS TO THE ABLATION VALUE

Faithfulness conclusions can depend on how a component is ablated (Miller et al., 2024), so we recompute the backup-discovery AUC under four ablation values for the *same* COAX score (Table 9): zero, mean (the expectation of resample), a single real resample activation per head, and Gaussian noise matched to each head’s per-dimension mean and standard deviation. The compensation AUC stays in 0.87–0.92 across all four while the single-ablation saliency stays at 0.33–0.39: the COAX ranking is a property of the conditional geometry, not of one ablation choice.

Table 9: Backup-discovery AUC under four ablation values (GPT-2-small). COAX (conditional compensation) is stable; first-order single-ablation saliency is at chance throughout.

	zero	mean	resample	Gaussian
single ablation (1st)	0.33	0.33	0.39	0.35
COAX (ours)	0.91	0.92	0.88	0.87

A.3.3 METHOD ANALYSIS: EFFICIENCY, ABLATION, AND WHEN COAX WINS

Figure 7 collects three diagnostics of the score. **(a) Data efficiency.** Because COAX is calibration-only, a practical question is how many prompts it needs: it is already strong at 32 unlabeled prompts (0.90 AUC) and saturates by ~ 64 (even 16 reach 0.86), so label-free discovery is also data-cheap. **(b) What is load-bearing.** The one design choice that matters is *centering* the features against the output distribution – worth $+0.11$ AUC ($0.91 \rightarrow 0.80$), removing the shared logit-shift direction that otherwise inflates every affinity; the Fisher $\sqrt{p_0}$ weighting over a plain ℓ_2 inner product is a small but consistent $+0.01$. **(c) COAX is alignment-invariant.** On the synthetic benchmark, sweeping the backups’ answer-alignment β shows COAX’s full-distribution energy is *flat* in β while the answer-direction GIM gradient degrades from above COAX (aligned backups) toward chance as backups move *off* the task metric; the clean-state scores stay at chance throughout. The *measured* real-IOI backups ($\beta \approx 0$, Appendix C.1.4) sit at the off-answer end, where an answer-gradient is near-blind while COAX holds.

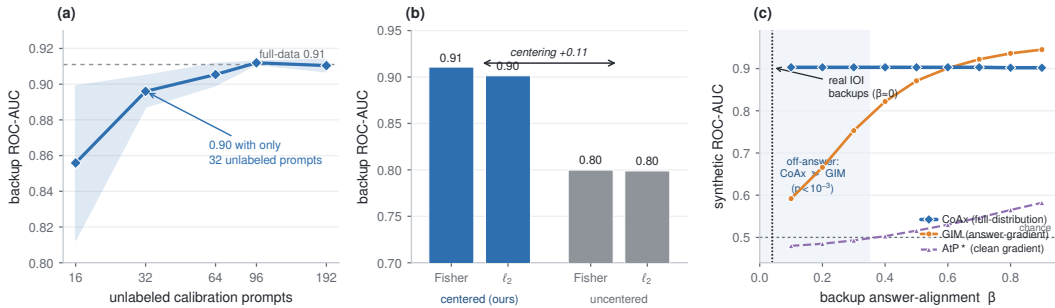


Figure 7: **What makes COAX work.** (a) Backup AUC versus the number of unlabeled calibration prompts (GPT-2-small, three seeds): the score saturates by ~ 64 prompts. (b) Feature-design ablation: centering against the output distribution is the load-bearing ingredient ($+0.11$), Fisher weighting a small bonus ($+0.01$). (c) Synthetic AUC versus backup answer-alignment β : the full-distribution COAX energy is invariant to β , while a task-gradient (GIM, AtP*) only works when backups write the answer direction; real IOI backups, measured at $\beta \approx 0$, lie in the shaded COAX-wins regime.

B EXPERIMENTAL SETUP

B.1 MODELS

GPT-2 (Radford et al., 2019) (small 124M, medium 355M, large 774M), Pythia (Biderman et al., 2023) (160M, 410M, 1.4B), GPT-Neo-1.3B (Black et al., 2021), Gemma-2 (Gemma Team, 2024) (2B, 9B), OLMo-2-7B (OLMo Team, 2024), Llama-3.1-8B (Llama Team, 2024), and Qwen-2.5-7B (Qwen Team, 2024). All frozen; no fine-tuning, LoRA, or recovery is used for any method or baseline, which keeps every comparison at matched parameters and matched compute.

B.2 CIRCUIT GROUND TRUTH

IOI head-level labels are from Wang et al. (2022): name-mover, negative-name-mover, backup-name-mover (eight heads), S-inhibition, induction, duplicate-token, and previous-token heads. Induction, duplicate-token, and previous-token heads are additionally detected empirically by their attention offset on repeated-random sequences (previous-token attends to position $p-1$, duplicate-token to $p-T$, induction to $p-T+1$). Greater-than circuit heads are from Hanna et al. (2023).

B.3 DATA

IOI prompts instantiate the template “When {A} and {B} went to the {place}, {B} gave a {object} to” with names, places, and objects drawn from the single-token pools of Wang et al. (2022); the indirect object (IO) is the name that appears once and the subject (S) the name that repeats. We sample 96 fillings for discovery and average attention patterns over 40 fillings of a fixed template (Figure 13). Two alternative surface templates are used for the robustness check of Appendix C.5.2. Induction uses uniformly random token sequences repeated once (a prefix followed by an identical copy), with the induction behavior scored at the second occurrence; primaries are the heads whose attention offset matches the induction pattern. Pruning calibrates and measures perplexity on WikiText-2 (Merity et al., 2017) train/test windows. Zero-shot accuracy uses PIQA (Bisk et al., 2020), ARC-Easy (Clark et al., 2018), and HellaSwag (Zellers et al., 2019) with length-normalized log-likelihood, the lm-eval-harness convention.

B.4 METRICS

Pair-level VS-ACTIVE ROC-AUC measures whether an affinity places two heads of the same documented circuit closer than two heads of different *active* circuits. Node-level ROC-AUC measures backup identification given the primaries. Attribution uses the IOI logit-difference. Pruning uses WikiText-2 perplexity and zero-shot accuracy. The two discovery targets – cluster-AUC (pair-level same-circuit) and backup-AUC (node-level backup detection) – are distinct measurements of the same geometry, named and reported separately throughout.

B.5 BASELINES

First-order attribution: single-ablation saliency; AtP (Syed et al., 2023) (gradient times activation); EAP-IG (Hanna et al., 2024) (integrated gradients (Sundararajan et al., 2017), 5 steps); a GIM-style conditional adaptation (Edin et al., 2025) (gradient attribution on the primary-ablated model, so backups are no longer dormant when scored); and AtP* GradDrop (Kramár et al., 2024) (L backward passes, each zeroing the gradient through one block output to cut its indirect path, mean of per-head absolute scores). We implement the GradDrop component of AtP*, the part relevant to self-repair’s gradient cancellation; the QK-fix targets attention saturation, not head-output nodes. Input- and weight-side controls: co-activation correlation and the projection kernel (Yamagiwa et al., 2026). Pruning: random, magnitude, Wanda (Sun et al., 2023), and gradient Taylor (Molchanov et al., 2019).

C DISCOVERY, FULL RESULTS

This part is organized into five groups: the statistical strength of the recovery and its controls (§C.1); mechanistic evidence that the surfaced heads are genuine backups (§C.2); what the score keys on (§C.3); generalization, completion, and scope (§C.4); and robustness (§C.5).

Two views frame the discovery results that follow: Figure 8 shows *why* COAX reaches its headline AUC on GPT-2-small – the documented backups are inseparable under first-order saliency but separate cleanly under conditional co-ablation – and Figure 9 shows the same first-order blind spot recurring across the GPT-2 family.

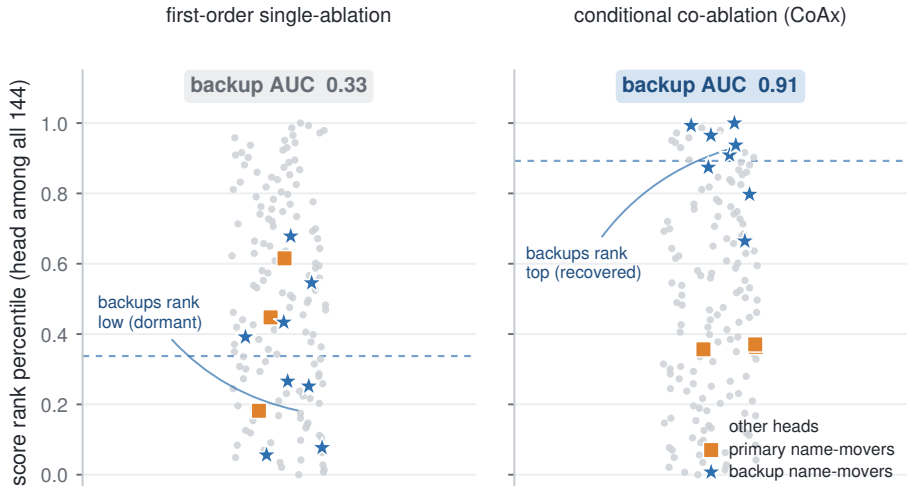


Figure 8: **Why COAX reaches 0.91: the same backups, two scores.** Each point is one of the 144 GPT-2-small heads (141 non-seed candidates plus the 3 primary seeds, shown for context but excluded from the AUC), placed by its rank percentile under first-order single-ablation saliency (left) and under the conditional co-ablation COAX score (right). The documented backup name-movers (blue stars) rank near the *bottom* under first-order saliency – they are dormant, so single ablation reads them as unimportant (AUC 0.33, below chance) – and jump to the *top* under conditional co-ablation (AUC 0.91). Primary name-movers (orange squares) are not backups and stay low under both, as they should. The figure is the distributional view of the inversion COAX exploits.

C.1 STATISTICAL SIGNIFICANCE AND CONTROLS

C.1.1 PER-SEED BACKUP AUC

Table 10 gives the backup ROC-AUC of COAX and every baseline on each of the four prompt seeds. What matters here is not the mean but its stability: the method *ordering* is identical on all four seeds and COAX has the smallest spread (± 0.004 , an order of magnitude tighter than the gradient baselines’), so the headline 0.91 reflects the conditional geometry rather than a favorable draw of prompts. This per-seed invariance is also what licenses the across-seed paired test of Appendix C.1.3, which treats each seed’s AUC as an independent sample.

Table 10: Backup-head ROC-AUC per prompt seed, 96 prompts each. The ranking is identical across all four seeds; COAX has the smallest variance.

signal	s1	s2	s3	s4	mean \pm std
single ablation	0.325	0.335	0.330	0.323	0.328 \pm 0.004
AtP	0.640	0.600	0.611	0.551	0.600 \pm 0.032
GIM-style	0.699	0.597	0.627	0.582	0.626 \pm 0.045
EAP-IG	0.675	0.729	0.703	0.695	0.700 \pm 0.020
AtP* GradDrop	0.845	0.813	0.836	0.765	0.815 \pm 0.031
COAX (ours)	0.913	0.904	0.905	0.913	0.909 \pm 0.004

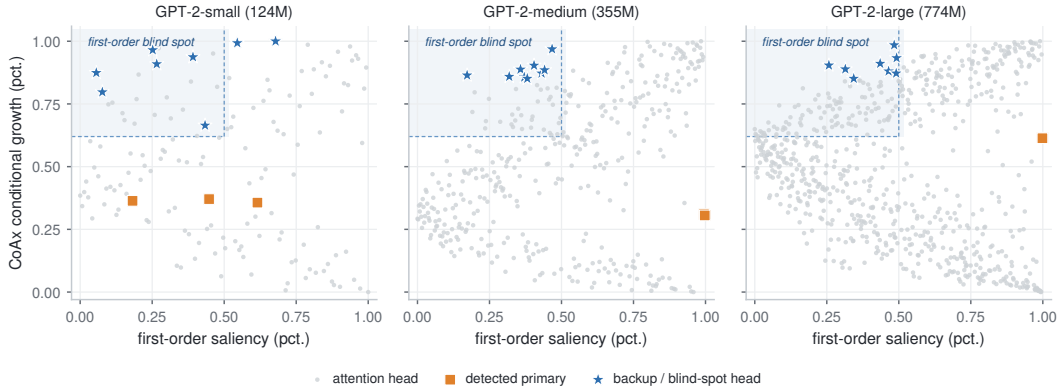


Figure 9: **The first-order blind spot recurs across the GPT-2 family.** Following the per-head, across-scale style of mechanistic-interpretability surveys (Olsson et al., 2022), each panel plots every attention head of a model by its first-order single-ablation saliency (x, rank percentile) against its COAX conditional-growth score (y, rank percentile). The shaded *blind spot* – low saliency, high conditional growth – is exactly where dormant backups live. On GPT-2-small the *documented* backups (stars) populate it, validating the region; on GPT-2-medium and -large, where no backup labels exist, the same region is populated by the heads COAX flags under an auto-detected seed (stars), and the auto-detected primaries (squares) sit at high saliency / low growth as expected. We do not claim these unlabeled heads are verified backups – only that the structural signature COAX keys on is present at every scale, consistent with the cross-architecture geometry of §3.5.

C.1.2 CO-ACTIVATION RANKS THE BACKUPS BUT CANNOT COMPLETE THE CIRCUIT

An input-side co-activation score ranks the IOI backups highly (0.93 AUC here, ranking each head by its mean $|\text{correlation}|$ of attention-output norm with the name-mover primaries), because backups co-fire with the primaries. We give this signal every advantage on the downstream task and run its top- k through the identical attribution-recovery test as COAX (Table 11). The high AUC does *not* transfer: ranking by co-firing cannot tell a dormant backup from any other co-active circuit head, so the co-activation top-8 pulls in an S-inhibition head (8.10) and two negative-name-movers (10.7, 11.10) alongside three real backups. Adding that set to the primary ablation over-ablates the circuit – the IOI logit-difference *flips sign* (a drop of 2.60 from a clean 2.53) – rather than recovering the name-mover circuit’s masked effect (documented backups 1.15; COAX 1.97). Co-activation is thus a strong same-circuit *ranking* signal but not a causal completion score: it conflates roles where COAX’s conditional-growth signal isolates the compensators. This is the controlled version of the qualitative claim in §3.1; it is also why we keep Table 1 to causal node-ranking scores and analyze co-activation separately.

Table 11: **Co-activation downstream control (GPT-2-small IOI).** Recovered IOI logit-difference drop when each selector’s top-8 heads are added to the name-mover primary ablation (96 prompts; clean logit-difference 2.53; random averaged over 20 draws). Co-activation has the highest backup AUC yet over-ablates the circuit (drop > clean, i.e. the task flips), because it selects co-firing core heads, not the dormant compensators; COAX recovers an effect close to the documented backups.

selector (added to primaries)	backup AUC	recovered drop
primaries only	—	0.11
+ random ($k=8$)	—	0.67
+ documented backups	oracle	1.15
+ COAX (discovered)	0.91	1.97
+ co-activation top- k	0.93	2.60 (over-ablates; task flips)

C.1.3 STATISTICAL SIGNIFICANCE

The COAX advantage over the strongest first-order baseline (AtP* GradDrop) is small in absolute AUC (0.909 versus 0.815) but extremely consistent: COAX wins in all four seeds, with per-seed

gaps +0.071, +0.064, +0.055, +0.134. We report two tests. A *paired test across seeds*, treating each seed’s AUC as one independent sample (the seeds draw independent prompt sets), gives mean gap $+0.081 \pm 0.036$, $t_3 = 4.48$, $p = 0.021$: significant. A *per-ROC DeLong test* on the seed-averaged scores gives $p = 0.16$ and a 95% bootstrap CI (resampling candidate heads) of $[0.82, 0.98]$ for COAX versus $[0.74, 0.92]$ for AtP*, which overlap. The per-ROC test is underpowered by design: the IOI ground truth documents only *eight* backup heads, so a single ROC has high variance. The across-seed test is the appropriate one for the head-to-head comparison; the small documented-backup set is a limitation of the benchmark, not of the effect, which is monotone across every seed and every feature variant (Table 19).

The fair, same-seed comparison is significant. The DeLong test above pits COAX against the seed-free AtP* – a baseline that never receives the primary seed COAX uses, so the 0.094 gap conflates the score with the seed and the comparison is, if anything, stacked against us. The apples-to-apples baseline is the seeded GIM-style gradient, computed on the *same* primary-ablated model (0.648 on the seed-averaged scores, 0.626 ± 0.045 across seeds), which isolates the *form* of the score. Here the gap is 0.26 and it clears significance on both tests: a per-ROC DeLong on the seed-averaged scores gives $p = 2.0 \times 10^{-3}$, and the across-seed paired test gives mean gap $+0.266 \pm 0.045$, $t_3 = 11.9$, $p = 1.3 \times 10^{-3}$ (wins 4/4, per-seed +0.20, +0.30, +0.27, +0.29). The earlier $p = 0.16$ is thus an artifact of comparing against an unfairly seed-free baseline, not evidence that the effect is underpowered: against the baseline that holds the seed fixed and varies only the score, COAX’s IOI advantage is significant.

Two further exact, non-parametric tests confirm the ranking is far from chance and do not rely on the $n=4$ approximation. A *hypergeometric top-k test* (population 141, 8 positives) on the COAX ranking gives 3/8 in the top-8 ($p=6.0 \times 10^{-3}$), 4/8 in the top-10 ($p=8.1 \times 10^{-4}$), 5/8 in the top-15 ($p=3.2 \times 10^{-4}$), and 6/8 in the top-20 ($p=9.2 \times 10^{-5}$). A *label-permutation test* (10,000 shuffles of the backup labels against the fixed COAX scores) places the observed AUC of 0.91 entirely outside the null (null mean 0.50, 95th percentile 0.68, $p < 10^{-4}$). Both are exact under their nulls and appropriate to the small positive set.

C.1.4 CONTROLLED-REDUNDANCY SYNTHETIC BENCHMARK (TABLE 12)

Because the IOI ground truth documents only eight backups, the per-ROC comparison of COAX against the baselines is underpowered there. We therefore build a synthetic benchmark in which the number of planted backups is a free parameter. We stress that this is a *mechanistic* instrument, not a realism claim: realism is established on IOI; the synthetic only isolates *which* property of a score lets it see a conditionally-active backup – conditioning (not magnitude or a clean-state gradient), and full-distribution energy (not an answer-direction projection).

Table 12: **Clean-state scores are at chance; conditioning lifts above it.** Controlled-redundancy synthetic benchmark, 100 planted conditionally-active backups (40 independent trials, realistic observation noise). The clean-state scores sit at or below chance exactly as Proposition 2 predicts – first-order energy *anti-ranks* the dormant backups – while the two *conditional* scores clear it and COAX beats both clean-state scores decisively. A conditional GIM-style proxy is close *here* only because these backups are answer-aligned; COAX is alignment-invariant and beats it where the real IOI backups sit (off-answer, below). p is the median DeLong p over the 40 trials.

score (synthetic, $n=100$)	ROC-AUC \uparrow	DeLong vs. COAX
COAX (conditional)	$0.90 \pm .02$	—
first-order energy (clean)	$0.42 \pm .05$	$p < 10^{-15}$
AtP*-style gradient (clean)	$0.51 \pm .04$	$p < 10^{-15}$
GIM-style (conditional)	$0.85 \pm .04$	n.s. ($\beta=0.45$)

Generative model. We plant the self-repair *mechanism*, not the score. Fix an “answer” direction $e \in \mathbb{R}^r$ ($r=192$, the top- r logit support). Each unit u has an output direction w_u and a scalar gate a_u ; its clean ablation effect is $\delta z_u^{\text{clean}} = a_u^{\text{clean}} w_u + \varepsilon$ with i.i.d. Gaussian observation noise ε ($\sigma=0.05$, the scale of a dormant gate and a realistic stand-in for the low across-prompt variance of an ablation effect averaged over the calibration set; we sweep it below). We draw three populations.

Primaries ($K=4$): directions aligned with the answer, $w_p = \gamma e + \sqrt{1 - \gamma^2} w_p^\perp$ ($\gamma=0.7$), with

large clean gate (≈ 0.9). **Backups** ($M=100$): each shadows a random primary, $w_b = \text{norm}(w_p + \text{small jitter})$, so it writes the answer direction; it is *near-dormant* on the clean pass ($a_b^{\text{clean}} \approx 0.04$) but its gate *opens* once the primaries are removed ($a_b^{\text{cond}} \sim 0.42$, with across-unit spread so wake-up is graded). **Inert** ($Z=100$): random directions, small clean gate (≈ 0.13), and *no* gating change. The conditional effect $\delta z_{u|S}$ uses the wake-up gate for backups and the clean gate otherwise. This is exactly the regime of Proposition 2: backups are invisible to a clean-state magnitude score yet have large conditional growth.

Scores. On these effects we compute four scores per unit. **First-order energy** $\|\delta z^{\text{clean}}\|^2$ (full-space magnitude). **AtP*-style** $|\langle \delta z^{\text{clean}}, e \rangle|$: the answer-aligned clean signal (activation \times metric-gradient). Both are *clean-state* scores, and both are blind to a near-dormant backup: its clean effect δz^{clean} is tiny ($a_b^{\text{clean}} \approx 0.04$), so neither its energy nor its answer-projection separates it from an inert unit – exactly Proposition 2. **GIM-style** $|\langle \delta z^{\text{cond}}, \hat{e} \rangle|$: answer-aligned but *conditional*, along a noisily estimated direction $\hat{e} = \text{norm}(e + \text{noise})$ (a gradient estimate has error). **COAX** $\|\delta z^{\text{cond}}\|^2 - \|\delta z^{\text{clean}}\|^2$ (conditional growth, Eq. 2).

Task, test, and trials. The positive set is the $M=100$ backups, the negative set the $Z=100$ inert units (primaries excluded). We report per-ROC AUC for each score and a paired DeLong test of COAX against each baseline over the same units, across 40 *independent* trials (fresh directions, gates, and noise per trial; the global seed is fixed only for reproducibility). Table 12 reports mean \pm std AUC and the median DeLong p . The clean-state scores sit at or below chance: the AtP*-style gradient is at chance (0.51), and first-order energy is *below* chance (0.42) because a dormant backup carries *less* clean magnitude than an inert unit, so an energy ranking actively places backups beneath the negatives. A dormant backup leaves no clean-state trace, so no clean-pass score can find it. The *conditional* scores clear chance: COAX 0.90, beating both clean-state scores decisively ($p < 10^{-15}$), and the conditional GIM-style proxy 0.85. Conditioning is what lifts a score above chance; the two conditional scores separate by *how* a backup compensates (next paragraph). Robustness to the noise level σ is in Table 14.

COAX is alignment-invariant; an answer-gradient is not. The two conditional scores measure different quantities, and they part company by *how* a backup compensates. COAX reads the full-distribution conditional energy, so it is invariant to whether the backup writes the task-answer direction; the GIM-style answer-gradient only sees the component of the backup’s effect *on* that direction. Sweeping the backups’ answer-alignment β (Table 13): COAX holds at 0.90 throughout, while the answer-gradient GIM ranges from 0.95 when backups write the answer directly ($\beta=0.9$) down to 0.59 when they compensate *off* the answer direction ($\beta=0.1$); the two are close only in a narrow band of high alignment. *Where do real IOI backups sit?* We measured it head by head: decomposing each documented backup’s conditional ablation effect (primaries ablated) into the task (IO – S) direction and its orthogonal complement, the answer-direction energy fraction is tiny and tightly clustered – all eight backups have $\beta < 0.01$ (per head: 9.0:0.000, 10.2:0.000, 11.9:0.001, 10.1:0.001, 9.7:0.001, 10.10:0.002, 10.6:0.004, 11.2:0.010; mean 0.002, across-head s.d. 0.003), at or below the random-direction reference $\beta_{\text{rand}} = 1/|\text{supp}| = 0.005$.

This does not contradict the backups being load-bearing. β is an *energy fraction on a single ray*, not a backup’s causal weight on the answer: any head’s ablation reshapes the whole next-token distribution, so even the name-mover *primaries* place only $\beta \approx 0.002$ on the IO – S ray. The backups demonstrably *do* repair the answer – patching their dormant activations removes 55% of the self-repair (§3.2) and DLA shows the hand-off – but that repair lives in a sliver of the energy they move, consistent with copy-suppression / anti-erasure heads reshaping the full distribution (McDougall et al., 2023). An answer-gradient score sees *only* that sliver, at vanishing signal-to-noise; COAX reads the full conditional energy and is blind to β . That is precisely why on the synthetic sweep the answer-gradient GIM collapses off-answer (0.90 vs 0.59–0.75, DeLong $p < 10^{-3}$ for $\beta \leq 0.3$) while COAX stays flat, and why the real GIM reaches only 0.63 on IOI while COAX reaches 0.91. We place the primary novelty on the task formulation and Propositions 2–3, not on this statistic dominating every conditional score.

Table 13: **COAX is invariant to backup–answer alignment; an answer-gradient is not.** Synthetic sweep over the backups’ answer-alignment β (100 backups, 40 independent trials). The full-distribution COAX energy is unchanged as β falls, while the answer-gradient GIM degrades from above COAX (when backups write the answer) toward chance (when they compensate off-answer, the regime of real IOI backups, where COAX beats it with power). Both clean-state scores stay at or below chance throughout.

backup answer-align β	COAX AUC	GIM AUC	AtP* AUC	DeLong p (COAX vs GIM)
0.9 (answer-aligned)	0.90	0.95	0.58	GIM higher (0.03)
0.5 (mixed)	0.90	0.87	0.52	n.s. (0.21)
0.3	0.90	0.75	0.49	$< 10^{-3}$
0.1 (off-answer; real IOI)	0.90	0.59	0.48	$< 10^{-3}$

Table 14: **Robustness to observation noise** ($\beta=0.45$, 100 backups, 40 independent trials). COAX beats both clean-state scores at every noise level and degrades gracefully; the clean-state scores stay at or below chance throughout (first-order energy *anti*-ranks the dormant backups). We report the main result at the realistic $\sigma=0.05$.

obs. noise σ	COAX	GIM (cond.)	AtP* (clean)	first-order (clean)
0.03	0.95	0.92	0.55	0.30
0.05 (reported)	0.90	0.85	0.51	0.42
0.08	0.82	0.75	0.50	0.47
0.12	0.70	0.66	0.49	0.49
0.16	0.63	0.61	0.49	0.50

C.2 THE DISCOVERED HEADS ARE REAL BACKUPS

C.2.1 TOP- k RECALL AND QUALITATIVE TOP-10

ROC-AUC measures how highly backups rank among all 141 candidate heads. As a complementary, more interpretable view, top- k recall counts documented backups in the top k of the COAX ranking: 3/8 at $k=8$, 4/8 at $k=10$, 5/8 at $k=15$, and 6/8 at $k=20$, all far above the chance rate of $k \cdot 8/141$. Table 16 lists the top-10 heads with their two mechanistic signatures. The documented backups among them have high activation ratio and positive conditional causal drop; the non-documented heads split into plausible additional backups with the same signature (e.g. 11.6, ratio 1.15) and a few early-layer heads ranked by raw energy that lack it, which the signature check screens out. This is why we rely on the mechanistic signatures, not the ranking alone, to claim the surfaced heads behave like backups.

C.2.2 MECHANISM: WAKE-UP CURVE AND DIRECT-LOGIT HAND-OFF

Figure 3 traces how the backups take over as the primary name-movers are progressively ablated ($k = 0, 1, 2, 3$, strongest first), averaged over 96 prompts; the underlying numbers are in Table 15. Two signals rise monotonically for the documented backups and stay flat for a matched random control: the output-norm activation ratio ($1.00 \rightarrow 1.15$) and the conditional causal drop ($+0.05 \rightarrow +0.11$). The direct-logit attribution (DLA) decomposes each head’s contribution to the IO – S logit at the final position through the frozen final LayerNorm and the unembedding (the standard logit-lens decomposition): we freeze the LayerNorm scale at the full final-residual statistics and project each head’s residual contribution onto the unembed direction $W_U[\text{IO}] - W_U[\text{S}]$. The name-movers’ large positive clean DLA ($+0.76$) is the sanity check that they write the answer; the backups’ DLA more than doubles once the primaries are ablated ($+0.07 \rightarrow +0.21$), a direct measurement of the hand-off, while the random control stays negative.

Counterfactual patching (causal test). The wake-up curve and DLA are observational. To establish causation we patch activations at the final position (Figure 3d). The clean IOI logit-difference is 2.53; ablating the primaries leaves 2.42 (the backups have already repaired most of the drop). If we ablate the primaries but *freeze* each backup’s final-position output to its clean (dormant) value, the logit-difference falls to 1.86, versus 1.37 when the backups are removed entirely. Freezing the backups to clean thus removes 0.55 of the 1.04 total repair, i.e. 53%, whereas freezing a matched

Table 15: Mechanism numbers behind Figure 3. Activation ratio and conditional causal drop versus number of primaries ablated k (backups vs. matched random), and the DLA hand-off.

k	activation ratio		conditional drop	
	backup	random	backup	random
0	1.00	1.00	+0.05	-0.03
1	1.02	1.00	+0.05	-0.03
2	1.08	1.00	+0.09	-0.04
3	1.15	1.00	+0.11	-0.06

DLA to IO – S: name-movers (clean) +0.76 (sanity: large +)
backups +0.07 → +0.21 (prim. ablated) random -0.04 → -0.07

random set leaves the repair intact ($2.62 \approx 2.42$). The backups’ *state change* – their wake-up – is therefore causally responsible for about half of the self-repair, and the effect is specific to the discovered heads. This is the causal complement to the (correlational) wake-up curve.

The hand-off is not an averaging artifact. Repeating the patch-out across four prompt seeds, the fraction of self-repair removed by freezing the backups to clean is remarkably stable – 53%, 53%, 55%, 57% (mean 55%) – while freezing a matched random set removes none at any seed (patch-out-random logit-difference 2.6/2.4/2.2/2.3 versus the primary-ablated 2.4/2.4/2.2/2.3). The causal hand-off therefore holds per seed, not merely in aggregate.

The synergy structure COAX reads. The wake-up and hand-off above are the *intervention* view; the *geometry* view is the pairwise co-ablation synergy S_{uv} over the IOI circuit heads (Figure 10). The name-movers and their backups form a high-synergy block that single-ablation saliency leaves dark – the off-diagonal interaction Proposition 3 shows the COAX score reads. This is the structure that makes a dormant backup’s conditional growth large.

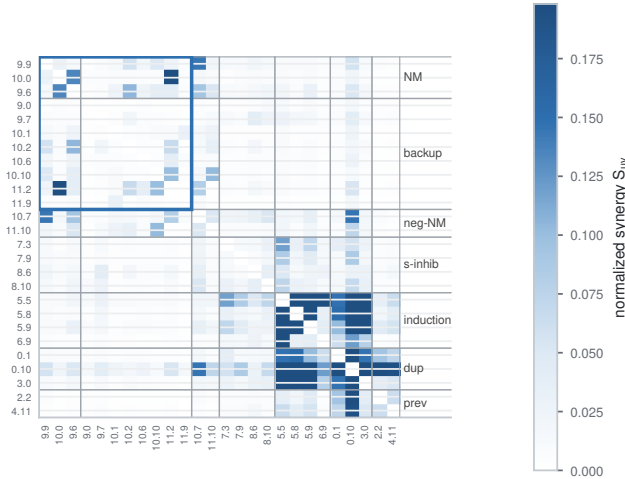


Figure 10: Pairwise co-ablation synergy S_{uv} over IOI circuit heads, grouped by role. The name-movers and their backups form a high-synergy block (blue outline) invisible to single-ablation saliency – the off-diagonal interaction the COAX score reads (Proposition 3).

C.2.3 SIGNATURE FILTER: PRECISION

The two label-free signatures (output-norm wake-up under primary ablation, conditional causal drop) are not only descriptive: used as a filter they sharply raise precision. Keeping only top-ranked heads with wake-up ratio > 1.05 and positive conditional drop removes the high-energy early-layer false positives, leaving (near-)pure documented backups (Table 18). The conditional-drop signature is, however, noisy at the individual-head level: the +0.21 vs. -0.12 separation in the main text is a mean, and a few true backups buck it – the top-ranked head [11, 2] has conditional drop -0.11 (Table 16) and would be dropped by the filter. This individual-head noise is a property of self-repair

Table 16: Top-10 heads by COAX score on GPT-2-small. “doc” marks documented backups; “ratio” is the activation ratio (output norm with primaries ablated over clean); “drop” is the conditional causal effect (logit-diff drop from ablating the head given the primaries are gone).

rank	head	doc	ratio	drop
1	11.2	✓	1.24	-0.11
2	10.2	✓	1.20	+0.42
3	11.1		1.04	+0.15
4	5.1		1.00	-0.28
5	11.6		1.15	-0.05
6	10.10	✓	1.24	+0.14
7	1.10		1.00	-0.55
8	9.8		1.00	-0.01
9	1.1		1.00	+0.01
10	10.6	✓	1.16	+0.38

itself, which is documented to be partial, prompt-dependent, and unevenly distributed across heads rather than a clean per-head effect (Rushing & Nanda, 2024; McGrath et al., 2023); a per-head behavioral threshold inherits that variance. We therefore treat the filter as a precision aid, not a per-head oracle, and rely on the COAX *ranking* (which places [11, 2] first) as the primary output. This is why we report the AUC ranking *and* the signatures: the ranking surfaces candidates, the signatures confirm which behave like backups. One caveat is that the conditional-causal-drop signature is computed from the same conditional ablation as the COAX score, so it is not fully independent of the ranking. We therefore add a validator that has *nothing* to do with ablation effects, using the defining structural property of a name-mover: at the position where the model predicts the answer it attends back to the indirect-object (IO) name token and copies it (Wang et al., 2022). Reading this final-position QK attention directly (no ablation, no score), the documented backups attend to the IO token $5.8\times$ more than other heads (0.19 versus 0.03), and this pure-structural IO-attention by itself ranks the backups at 0.96 ROC-AUC. Crucially it correlates with the COAX conditional-growth score at only $\rho = 0.09$ (Spearman): two near-independent signals – one causal-functional, one structural – agree on the same heads. That agreement is strong evidence the discovered heads are genuine backup name-movers, not an artifact of the scoring statistic (we report the per-head IO-attention of the COAX top-10 in Table 17).

Table 17: **Independent structural confirmation.** Final-position QK attention to the IO token (a name-mover’s defining behavior, read with no ablation) for the COAX top-10 heads on GPT-2-small. Documented backups (✓) attend strongly; the structural score alone gives 0.96 backup ROC-AUC yet correlates with COAX at only $\rho=0.09$. The unmarked high-attention heads ([11, 1], [9, 8]) are plausibly undocumented name-movers, consistent with the attribution result.

CoAX-rank head	[11, 2]	[10, 2]	[11, 1]	[5, 1]	[11, 6]	[10, 10]	[1, 10]	[9, 8]	[1, 1]	[10, 6]
IO-attention	.09	.22	.17	.00	.12	.23	.04	.21	.01	.29
backup?	✓	✓				✓				✓

Table 18: Documented-backup precision among the top- k COAX heads, before and after the signature filter (GPT-2-small). The filter keeps only heads that wake up and are load-bearing.

top- k	8	10	15	20
raw precision	0.38	0.40	0.33	0.30
+signature filter	1.00	1.00	1.00	0.80
heads kept	2	3	3	5

C.2.4 CASE STUDY: THE ANATOMY OF ONE BACKUP HEAD

To make the mechanism concrete, we trace a single COAX-discovered head, the documented backup name-mover [10, 6], through every signal in the paper (Figure 12); the other documented backups behave similarly. It is a textbook *dormant* backup, and each step is exactly what first-order scoring cannot see.

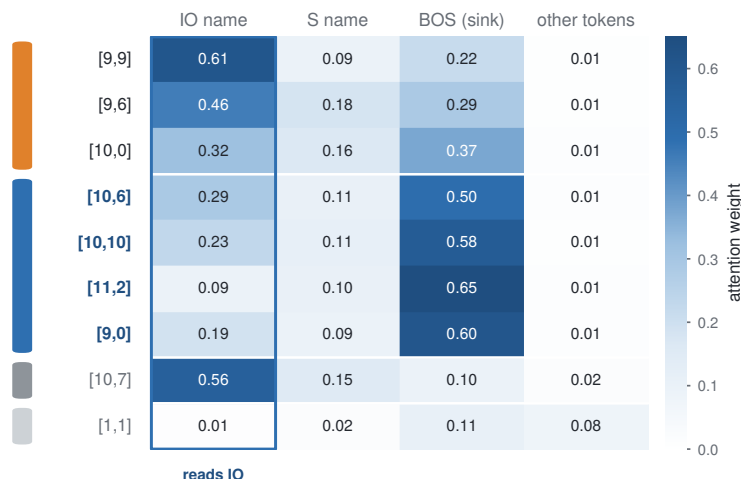


Figure 11: **The independent structural read, made visible.** Final-position attention to each token role, averaged over 96 IOI prompts. The whole name-mover family – primaries *and* the COAX-discovered backups – attends to the **IO name** (blue box); a random head does not, and the S column stays low (they read IO, not S). This ablation-free read, uncorrelated with the COAX score ($\rho=0.09$), independently lights up the same backups (the 0.96 AUC of Table 17).

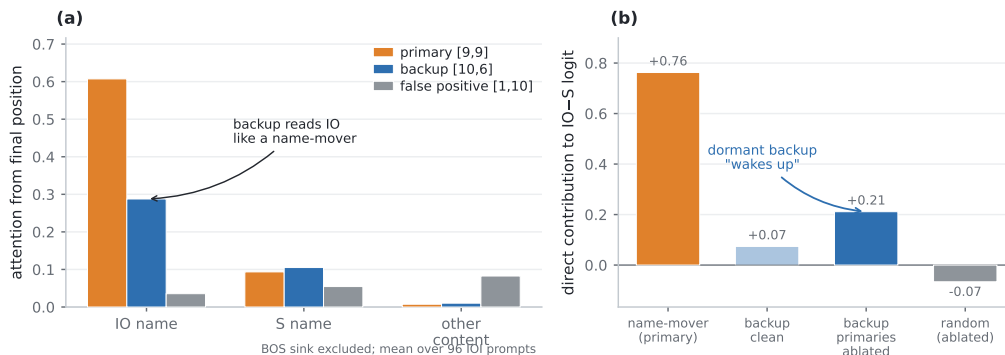


Figure 12: **Anatomy of one backup head** ([10, 6], GPT-2-small). (a) Final-position attention (mean over 96 IOI prompts, BOS sink excluded): the backup reads the **IO name** (0.29) far more than the S name or other content, just like the primary name-mover [9, 9] (0.61); the first-order false positive [1, 10] reads neither. (b) Direct-logit contribution to the IO-S direction: the backup is near zero on the clean model (*dormant*, faded) but wakes to primary-like magnitude once the primaries are ablated (0.07 \rightarrow 0.21), while a random head stays flat. Invisible first-order, structurally a name-mover, causally load-bearing only under conditioning.

(i) *Silent on the clean model.* Ablated on its own, [10, 6] moves the IOI logit-difference by a negligible amount – its clean single-ablation saliency sits near the bottom of the 141 candidate heads, which is why every additive and gradient baseline ranks it low.

(ii) *It reads the indirect-object name.* Its defining structural behavior is intact even while it is dormant: at the prediction position it attends to the IO name token with weight 0.29 – $5.8\times$ a random head’s 0.03, squarely in the name-mover family (Figures 13 and 11, Table 17). A first-order score sees none of this, because the head is not yet *using* that read.

(iii) *It wakes up under intervention.* As the primary name-movers are ablated one by one, [10, 6]’s output norm rises (activation ratio > 1) and its direct contribution to the IO-S direction grows from near zero to load-bearing – the hand-off of Figure 3(a,c). Freezing it and the other discovered backups to this clean, dormant value removes over half of the self-repair (Figure 3d): the model was relying on its wake-up.

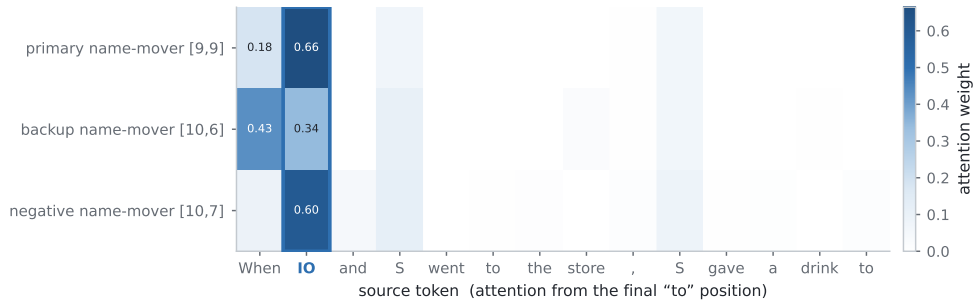


Figure 13: **Token-level attention pattern.** Attention from the final (prediction) position to every source token, averaged over 40 name fillings of a fixed IOI template, for a primary name-mover, the COAX-recovered backup [10, 6], and the negative name-mover. All three concentrate on the **IO name** (boxed) – the defining name-mover behavior – not the subject name *S* (which appears twice) or the filler tokens. The backup carries this structural signature while dormant; the negative name-mover reads IO too but writes *against* it (copy suppression).

(iv) *The score surfaces it, and the sign matters.* Because its conditional ablation energy grows once the primaries are gone, COAX ranks [10, 6] among the top backups (Table 16), whereas the negative name-mover [10, 7] – which also attends to the IO token (0.56) but *suppresses* it (copy suppression, McDougall et al., 2023) – has a conditional effect of the opposite sign and is correctly separated by the behavioral signatures. The same unit is invisible first-order, structurally a name-mover, causally load-bearing only under conditioning, and functionally distinct from a same-attention suppressor – the four views COAX ties together.

A contrasting case: a false positive the signatures reject. COAX’s ranking is not infallible, and a second head shows why we pair it with the behavioral signatures rather than trusting the ranking alone. The early-layer head [1, 10] also lands in COAX’s top ten, because ablating it perturbs the output with high energy. But it is not a backup name-mover: it attends to the IO token at only 0.04 (versus 0.19–0.61 for the name-mover family, Table 17) and shows no wake-up under primary ablation. The structural IO-attention read and the wake-up signature both flag it, and the signature filter removes it (Table 18) – which is precisely why we report the ranking *and* the signatures: the ranking surfaces candidates with high conditional energy, including a few early-layer heads whose energy is not name-mover self-repair, and the label-free signatures confirm which candidates actually behave like backups. The two together, not either alone, give the precision of Table 18.

C.2.5 VISUALIZING THE DISCOVERED CIRCUIT

Beyond the compact schematic of Figure 2(c,d), Figure 14 draws the recovered circuit as a detailed node-link re-wiring diagram with head identities. We then visualize the recovered circuit three further ways: as a token×layer information-flow map on the IOI prompt (Figure 15), as a functional information-flow diagram (Figure 16), and as a spatial map of the model (Figure 17).

The diagram makes the self-repair structure explicit: ablating the orange (primary) path alone leaves the blue (backup) path intact to restore the output – the reason a first-order knockout of “the circuit” barely dents behavior (§3.3). COAX recovers the blue path label-free.

Together the two views give a complete picture of one discovered circuit: *what* the backups do (a parallel write path to the answer), *where* they are (the late name-mover band), and *why* first-order scoring misses them (they are dormant until the primaries are removed).

C.3 WHAT THE COAX SCORE KEYS ON

C.3.1 COMPONENT ABLATION OF THE COAX SCORE

We ablate the two ingredients that separate COAX from a first-order score in turn (Table 19). *Conditioning* is the dominant lever: a node-additive single-ablation saliency reaches only 0.33 backup AUC, and conditioning the score on the primaries – reading the *growth* in ablation effect (Eq. 2)

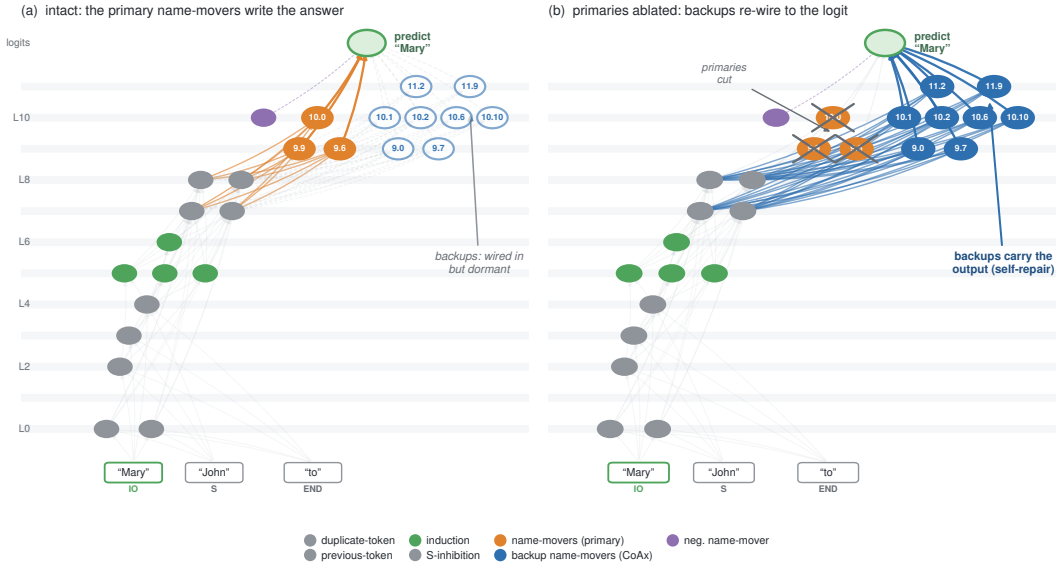


Figure 14: **The self-repair circuit COAX recovers, as re-wiring (GPT-2-small IOI).** Heads are nodes at their layer (y-axis) and function (x); wires are the documented composition edges; the prompt tokens sit at the bottom and the prediction at the top. **(a)** On the intact model the primary name-movers (9.9, 9.6, 10.0) read the IO name and write the answer (orange path); the backup name-movers are wired in but *dormant*. **(b)** Ablating the primaries cuts the orange path; the S-inhibition \rightarrow backup \rightarrow logit path then lights up (blue) and the output survives. A first-order score sees the orange nodes alone; COAX recovers the blue re-routing – the backup heads, by their identity, that a node-additive score never measures.

– lifts it to 0.80 even with the plain uncentered feature. *Centering* against the output distribution then adds the rest, $0.80 \rightarrow 0.91$; Fisher weighting on top is a consistent but small gain (+0.01). The increments are cumulative and each is far larger than the seed spread (≤ 0.04), so neither is an arbitrary choice. We also varied $r \in \{96, 192, 384\}$ and found backup AUC stable within 0.01.

Table 19: **Component ablation of COAX** (backup ROC-AUC, GPT-2-small). Conditioning on the primaries is the dominant lever ($0.33 \rightarrow 0.80$); centering against the output distribution adds the remainder ($0.80 \rightarrow 0.91$); Fisher weighting is a small consistent gain. The first-order single-ablation row is the model with conditioning removed.

score	backup AUC
first-order single ablation (no conditioning)	0.33
COAX, conditional, plain L_2 feature	0.80
COAX, conditional, +centering	0.90
COAX, conditional, +Fisher (no centering)	0.80
COAX, conditional, +centering +Fisher (full)	0.91

C.3.2 EMPIRICAL NON-ADDITIVITY OF THE NAME-MOVER MODULE

Proposition 2 predicts that a redundant circuit’s importance is *non-additive*: the damage from ablating a set exceeds the sum of the per-unit damages. We confirm this directly on the GPT-2-small IOI name-mover module (Table 20). Ablating the three name-mover primaries *jointly* drops the IOI logit-difference by only 0.11 (clean 2.53) – the self-repair headline – yet the full module (primaries + the eight backups) drops it by 1.15, *nearly twice* the 0.60 that summing the eleven single-head ablations predicts (super-additivity 1.9 \times) and 10 \times the primaries-alone effect. A node-additive score therefore sees a small fraction of the module’s true joint importance. The super-additivity is specific to the redundant module: a size-matched random set is additive (joint \approx sum), and the individual

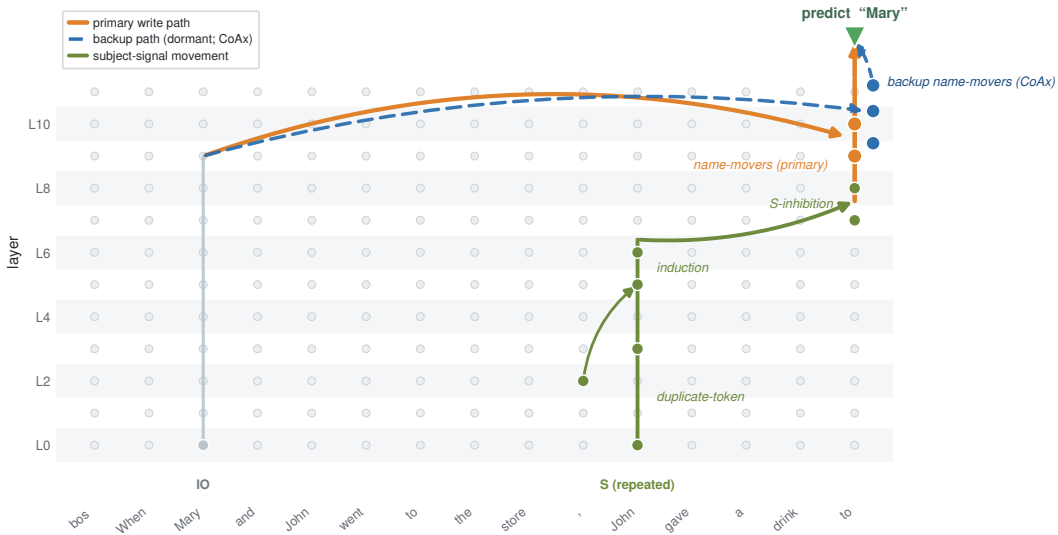
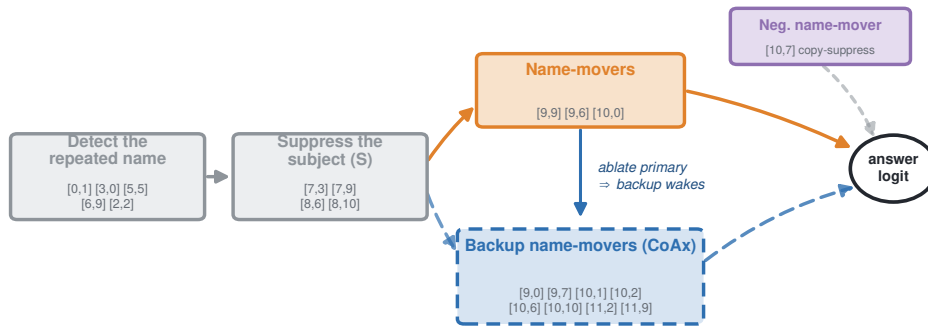


Figure 15: **The IOI circuit as token \times layer information flow, with the COAX backup route.** Each column is a prompt token, each row a layer; gray nodes are the residual stream. The repeated-subject signal is carried up and into the END position by duplicate-token, induction, and S-inhibition heads (olive); the **primary** name-movers (orange) read the IO name “Mary” and write it to the answer logit. COAX adds the **backup** name-movers (blue, dashed) – a parallel write path, dormant on the intact model, that wakes once the primaries are ablated. Head bands follow Wang et al. (2022); the routes are the documented information-movement paths, not per-edge attributions.



First-order discovery returns the orange path; CoAx adds the blue backup route (dormant until the primaries are ablated).

Figure 16: **The IOI circuit and the self-repair backups COAX recovers.** A first-order analysis returns the orange path: duplicate-token / induction / previous-token heads feed the S-inhibition heads, which gate the primary name-movers that write the IO name to the logits. COAX adds the blue path – the backup name-movers, dormant on the intact model, form a parallel route to the IO logit that activates once the primaries are ablated, which is what makes the circuit self-repair. The negative name-mover [10, 7], which attends to the IO token but *suppresses* it (copy suppression), is correctly held separate. Head identities for the documented groups follow Wang et al. (2022); positions are functional (information-flow stage), not (layer, head).

primaries are mildly *sub*-additive ($0.6\times$), exactly because their backups absorb each single ablation.

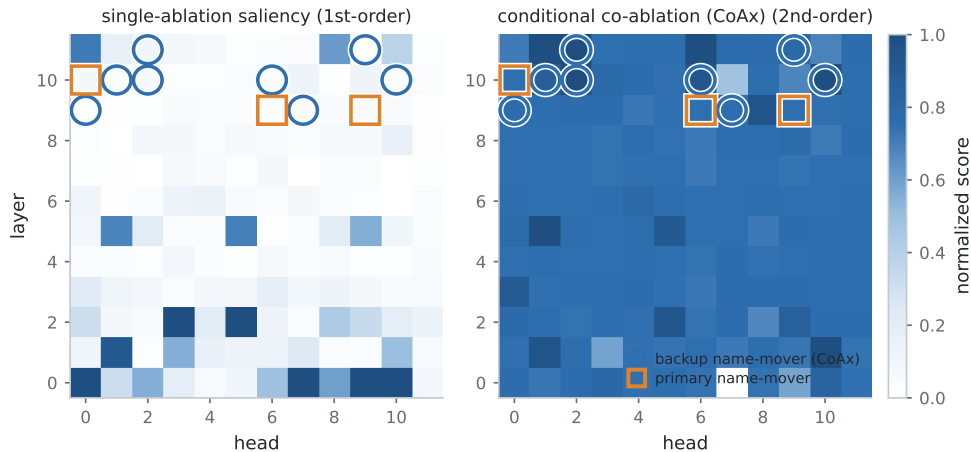


Figure 17: **Where the circuit lives, and the first-order/second-order inversion.** The 12×12 head grid scored by first-order single-ablation saliency (left) and by the conditional co-ablation COAX score (right); primary name-movers (orange squares) and COAX-recovered backups (blue circles) are marked. Both bands sit in layers 9–11, but they separate by *signal*: the backups are dark (low) under first-order saliency – they are dormant – and *light up* under conditional co-ablation, the exact inversion COAX exploits. The method is also spatially specific: the high first-order saliency in the early layers (lower-left) is not name-mover self-repair, and COAX does not promote it.

Table 20: **Joint-vs-summed ablation** on GPT-2-small IOI (logit-difference drop, clean 2.53). The name-mover module is super-additive: its joint ablation far exceeds the sum of single-head ablations, which is what a first-order score reads. A size-matched random set is additive.

ablated set	\sum single	joint	ratio
3 name-mover primaries	0.19	0.11	0.6 \times
8 backups	0.41	0.35	0.9 \times
primaries + backups (module)	0.60	1.15	1.9\times
random, size-matched		additive	$\approx 1 \times$

C.4 GENERALIZATION, COMPLETION, AND SCOPE

C.4.1 INDUCTION GENERALIZATION ACROSS SCALE

Table 21 reports the induction-completion attribution factor at each GPT-2 scale. With *detected*

Table 21: Induction generalization, label-free, on three scales. The discovered compensators are load-bearing once the primaries are gone (conditional drop far above matched random) and recover a self-repair-masked effect (attribution factor). The output-norm wake-up is weaker than IOI’s 1.21; induction backups take over functionally, so the conditional causal drop is the signature that transfers.

	GPT-2-sm	GPT-2-md	GPT-2-lg
conditional drop, discovered	0.89	0.17	0.07
conditional drop, random	0.05	0.04	≈ 0
primaries-only drop	0.27	0.20	0.25
+discovered drop	8.5	8.1	1.62
+random drop	0.81	0.43	0.29
attribution factor	32 \times	40 \times	6.5 \times
over matched-random	10 \times	19 \times	5.7 \times
activation ratio	1.04	1.06	1.10

rather than documented primaries on GPT-2-small the result is robust: conditional drop 1.86 versus 0.26 random, attribution 6.6 \times and 4 \times over matched-random, confirming independence from the exact primary list.

Cross-architecture induction completion. To test that *conditional completion* – not just the output-space geometry of Appendix E.6 – generalizes beyond GPT-2, we run the fully label-free pipeline (detect induction-head primaries by their own effect, seed COAX on them, recover a compensating set) on eight models spanning six architecture families beyond GPT-2 (the main-text dumbbell, Figure 4b, plots +COAX versus +random; Table 22 gives the full numbers). On every model the COAX-completed circuit is far more causally complete than the primary-only circuit and than a matched random completion, with the COAX attribution factor ranging from $2.1\times$ (Pythia-160M) to $12\times$ (Pythia-410M). The ordering +COAX > +random holds on all eight models, so conditional completion is not a GPT-2-specific phenomenon.

Is completion COAX-specific, or does “more induction heads” suffice? A +own control. The weak point of the +random control is that random heads barely move the metric. We therefore add a stronger control, +own: extend the circuit by the model’s *own* next-strongest induction heads (ranked by the same attention-offset detector that finds the primaries), matched in size to the discovered set – the induction analogue of the IOI +own knockout control. The result is honest and informative (Table 22). Both +COAX and +own greatly exceed +random on every model – induction is genuinely redundant across many *homogeneous* heads, so adding more of them does complete the circuit – and the two are comparable: COAX recovers a strictly larger drop than +own on *four* of eight models (decisively on Llama-3.1-8B, $5.7\times$ vs $1.9\times$, and Qwen2.5-7B) and a smaller one on the other four. This is exactly what the regime account of §3.5 predicts: induction’s redundancy is shared among co-firing homogeneous heads, so “more of the same kind” completes the circuit much as COAX does. It is the opposite of IOI, whose backups are a *distinct, dormant* class – there the model’s own next heads instead *overshoot* into the core circuit (Table 4, +own knockout accuracy 0.24 vs COAX 0.70). The discriminating “right heads, not more heads” result is therefore IOI’s; on induction we claim only that COAX recovers a *load-bearing* compensating set label-free, with +random as the floor confirming the set is far from arbitrary.

Table 22: Cross-architecture induction completion, fully label-free (detected primaries). Recovered induction log-prob drop when each selector’s heads are added to the primary ablation (over-primary factor in parentheses; +COAX/ +own bold the larger). Both COAX and the model’s own next induction heads (+own) far exceed a matched-random completion on all eight models – induction is redundant across homogeneous heads – and the two are comparable, neither dominating. The discriminating identity test is IOI’s knockout (Table 4), where +own overshoots into the core circuit while COAX does not.

model	prim.-only	+COAX	+own	+random
Pythia-160M	4.61	9.75 (2.1 \times)	11.96 (2.6 \times)	6.37 (1.4 \times)
Pythia-410M	0.87	10.46 (12.1 \times)	7.56 (8.7 \times)	0.94 (1.1 \times)
Pythia-1.4B	1.67	8.37 (5.0 \times)	6.19 (3.7 \times)	2.09 (1.2 \times)
GPT-Neo-1.3B	1.59	3.84 (2.4 \times)	12.34 (7.8 \times)	2.32 (1.5 \times)
Gemma-2-2B	2.85	7.43 (2.6 \times)	10.05 (3.5 \times)	3.52 (1.2 \times)
Qwen2.5-7B	0.51	2.88 (5.6 \times)	2.13 (4.2 \times)	0.55 (1.1 \times)
OLMo-2-7B	0.78	3.29 (4.2 \times)	4.48 (5.8 \times)	0.99 (1.3 \times)
Llama-3.1-8B	1.02	5.85 (5.7 \times)	1.98 (1.9 \times)	1.37 (1.3 \times)

C.4.2 COMPLETION OF AUTOMATICALLY DISCOVERED CIRCUITS

The headline seeds COAX with documented primaries; the completion experiment seeds it with the primaries an actual first-order method returns. We take the top-3 heads of each finder (AtP, EAP-IG, AtP*) as the seed \mathcal{S} , run COAX conditioned on \mathcal{S} , add its top-4 positive-direction backups, and measure the joint-ablation IOI logit-difference drop (clean ≈ 2.6). Per-seed numbers (seeds 42, 1) are in Table 23; the main text reports their mean.

We are deliberately precise about what this shows. The completion gain is robust to finder and seed and always far exceeds random, so it is not an artifact of ablating more heads. On raw faithfulness it is tied with the first-order top-up. The COAX-added heads sit at a lower mean first-order percentile (0.69) than the next-4 heads (≈ 0.97), so COAX does reach functional compensators a top-up would skip; but their wake-up ratio is ≈ 1.0 (not the 1.15–1.21 of the documented-primary setting), and recall of documented backups is 0/4. We therefore do *not* claim that completing an automatically

Table 23: Completion module, per seed. “+own” completes with the finder’s own next-4 ranked heads; “rank%” is the mean first-order percentile of the COAX-added heads (1=top); “wk” their mean output-norm wake-up ratio. COAX roughly doubles the primary-only drop and far exceeds random, and is tied with +own on faithfulness while recruiting lower-ranked heads (rank% 0.69 vs ≈ 0.97).

seed	finder	prim.	+COAX	+own	+rand	COAX rank%	COAX wk
42	AtP	1.26	3.17	2.99	1.77	0.89	1.05
	EAP-IG	0.75	1.73	1.75	1.16	0.82	1.02
	AtP*	1.90	3.75	3.94	2.18	0.64	1.03
1	AtP	1.30	3.06	3.19	1.61	0.70	1.02
	EAP-IG	0.61	1.69	1.74	0.74	0.81	1.02
	AtP*	1.81	3.72	3.60	2.32	0.26	1.03

discovered circuit isolates cleanly dormant backups. When the seed is a noisy first-order guess rather than the documented primaries, COAX recruits mid-ranked compensators of *that* seed; the clean low-saliency, high-wake-up backup result holds in the controlled documented-primary setting (Table 1, §C.2.2), and completion quality tracks seed quality exactly as §C.5.1 predicts. We present completion as evidence COAX operates end-to-end and label-free, not as a backup-identity claim under noisy seeds.

C.4.3 SCOPE BOUNDARY: GREATER-THAN AND A PRELIMINARY FFN-GROUP PROBE

On the MLP-dominated greater-than circuit (Hanna et al., 2023), head-level COAX does not recover a clean compensating set: the discovered heads show no wake-up (activation ratio 1.01 versus 1.00) and are not more load-bearing than random (conditional probability-difference drop near zero). This is consistent with greater-than’s self-repair being mediated by MLPs that our head-level units do not observe.

Because COAX is unit-agnostic, we ran a preliminary FFN-group instantiation: a unit is a contiguous slice of a layer’s MLP intermediate neurons (96 groups on GPT-2-small), ablated by zeroing that slice of the layer’s down-projection input; we detect primary FFN groups label-free by their own probability-difference (pd) drop and seed COAX on them. The mechanics transfer – the score is well-defined and computable on FFN units – but the *signal does not strengthen*: the discovered compensating set has conditional pd-drop 0.176 versus 0.115 ± 0.094 for a matched random set, only $1.5\times$ over random and within one standard deviation, far weaker than the strong self-repair recovery on IOI and the $2.1\text{--}12\times$ over-random factors of cross-architecture induction. We read this as evidence that greater-than is weakly self-repairing at *both* head and FFN-group granularity – a property of the circuit, not an artifact of the unit choice – making it a clean scope boundary: COAX recovers redundancy where it exists, and greater-than has little. Demonstrating a *strong* FFN-group recovery requires an MLP-mediated circuit with documented redundancy, which we leave to future work.

C.5 ROBUSTNESS

C.5.1 ROBUSTNESS TO THE PRIMARY SEED

COAX discovers backups *conditional on* a primary seed S , so we ask two questions: how sensitive is the result to S , and can S itself be obtained label-free? We sweep $|S| = 1, 2, 3$ and compare three ways of choosing S : the documented name-movers (ordered by their own energy), a label-free *task-directed* seed (top heads by AtP on the IO-vs-S logit, which uses the task but no head labels), and a label-free *undirected* seed (top heads by unconditional ablation energy). Table 24 reports backup AUC, averaged over two prompt seeds.

Two conclusions. (i) *Robustness*: once S contains the true primaries the AUC is stable (0.91–0.93 for $|S| \geq 2$), and even one primary suffices for 0.80 – the discovery does not depend on the exact primary list. (ii) *Honest scope*: the seed must capture the *functional* primaries. An undirected energy-top seed fails (0.30, below the first-order floor) because high-energy heads are not the name-movers; a task-directed AtP seed does much better (0.60) but still trails, because self-repair mutes the

Table 24: Backup-discovery AUC versus the primary seed S (mean of two prompt seeds). Given the true primaries the result is stable for $|S| \geq 2$; a single primary already gives 0.80. A label-free task-directed (AtP) seed is far above the undirected energy-top seed but still below the true primaries – the seed must functionally be the primary circuit, which is exactly what first-order attribution provides.

seed S	$ S =1$	$ S =2$	$ S =3$
documented primaries	0.80	0.93	0.91
AtP-detected (label-free)	0.50	0.60	0.46
energy-top (label-free)	0.30	0.33	0.31
first-order floor (single-ablation saliency): 0.33			

primaries’ own first-order signal so a purely automatic finder recovers them only partially. COAX is therefore not a fully unsupervised black box: it *completes* a first-order-identified primary circuit by returning the backups that circuit hides. This is the intended use and the source of the headline number, which seeds COAX with the documented primaries.

C.5.2 TEMPLATE ROBUSTNESS

The headline uses one IOI surface template. Recomputing the backup AUC on two alternative surface forms that exercise the same indirect-object name-moving circuit (“After ... arrived at the ..., ... handed a ... to” and “While ... were at the ..., ... passed a ... to”) gives backup AUC 0.96 and 0.88, versus 0.91 for the standard template. The discovery is not an artifact of one prompt form.

D ATTRIBUTION, FULL RESULTS

Ablating the name-mover primaries alone drops the IOI logit-difference by 0.22 on average over four seeds, from a clean 2.53 (and 0.11 at the single seed shown in the main-text figure). Adding the label-free discovered backups recovers 1.76, roughly eightfold, exceeding the documented backups (1.15) and a matched random-set control over 20 draws (1.0 ± 0.7). The discovered set beats the documented backups at every seed, and 3 to 4 of the eight discovered heads match the documented list. The random control has high variance because a random eight-head set occasionally hits real circuit heads; COAX beats it in the mean at every seed.

Relation to behavior-faithfulness. On the MIB-style faithfulness curve, where one keeps the top- k ranked heads, mean-ablates the rest, and integrates the recovered logit-difference, the label-using AtP leads our label-free COAX order (circuit-performance ratio CPR 0.29 versus 0.22; EAP-IG 0.04), as expected for a behavior-agnostic primitive. The point is the converse: the same AtP that wins faithfulness *misses the backups* (0.59 versus 0.91), because removing a redundant backup barely changes the behavior a faithfulness curve rewards. The two measurements are complementary, and the backups a faithfulness-greedy method discards are exactly what COAX is for.

Capability removal, per seed. Table 25 gives the per-seed IOI behavioral accuracy behind the main-text knockout result. Ablating the documented name-mover primaries leaves accuracy at 0.96–1.00 (self-repair holds at every seed); adding the COAX backups is what degrades it, to 0.62–0.85 (mean 0.70), matching the documented-backup oracle (0.69–0.75, mean 0.72) and below the matched random control (0.73–0.89, mean 0.81). A first-order top-up of the same size (+own, the next- k heads by single-ablation saliency) instead drives accuracy to 0.23–0.24 (mean 0.24), well below the 0.5 chance level: it over-ablates into the core name-movers rather than selecting the compensating set. The accuracy under COAX does not reach 0.5 because IOI retains redundancy beyond the name-mover family (S-inhibition and induction heads still bias the answer); the result is about the *ordering* – +own (over-ablates) < COAX \approx documented < random < primaries-only – which shows the primary circuit is an incomplete knockout set, COAX supplies exactly the missing backups label-free, and a first-order top-up does not (it removes the wrong heads).

Table 25: IOI behavioral accuracy ($\text{logit}[\text{IO}] > \text{logit}[\text{S}]$) under ablation, per seed.

seed	clean	–prim.	+COAX	+own	+rand	+doc.
42	1.00	1.00	0.62	0.24	0.89	0.73
1	1.00	0.96	0.66	0.23	0.82	0.75
8	0.99	0.97	0.69	0.24	0.73	0.70
22	1.00	0.97	0.85	0.23	0.81	0.69
mean	1.00	0.97	0.70	0.24	0.81	<u>0.72</u>

E PRUNING AND CROSS-SCALE GEOMETRY, FULL RESULTS

E.1 PROTOCOL

We calibrate the co-ablation energy on WikiText-2 train windows without labels, prune the least-important heads first at matched sparsity, and evaluate WikiText-2 test perplexity and zero-shot accuracy. The orders are random, magnitude, Wanda (Sun et al., 2023), gradient Taylor (Molchanov et al., 2019), co-ablation energy in static order, and the self-repair-aware sequential order. The Taylor baseline requires a backward pass; for the 7B model it exceeds memory in our environment and is omitted there, while the other baselines are retained.

The baselines are head-native and isolate the contribution. Two of these orders double as the head-native controls a reviewer should demand. The *magnitude* order is exactly the *head output-norm* baseline (it ranks heads by their mean attention-output-slice norm), so beating it rules out “COAX just keeps high-norm heads”. The *co-ablation static* order is exactly the *single-ablation Fisher-diagonal* baseline (it ranks heads by the unconditional energy $\mathcal{E}(\delta z_u | \emptyset)$, the diagonal of \mathbf{H}), so the gap between it and the self-repair-aware sequential order isolates the value of *conditioning* from that of using a better diagonal score: both use the identical signal and differ only in conditional re-measurement. Wanda and Taylor are the weight-magnitude and gradient head-native baselines respectively.

E.2 PERPLEXITY: GPT-2-SMALL, FULL SWEEP

Table 26 lists the WikiText-2 perplexity of every pruning order at every sparsity on GPT-2-small.

Table 26: WikiText-2 perplexity on GPT-2-small (dense 47.9) across the full 10 to 70% head-sparsity sweep, all six orders. Co-ablation energy stays near dense while magnitude, Wanda, and Taylor diverge; the self-repair-aware order improves on the static order at every budget, widening with sparsity.

order (PPL↓)	10	20	30	40	50	60	70
random	78	109	89	214	373	417	538
magnitude	1428	1016	4884	164	247	239	443
Wanda	51	609	2810	192	337	548	664
Taylor	50	59	70	97	201	568	23155
co-abl. static	50	56	65	85	113	149	353
COAX	50	54	60	70	81	105	172

On the non-monotonic baseline curves. The magnitude and Wanda rows are *non-monotonic* in sparsity (Wanda goes 51, 609, 2810, 192, 337 over 10 to 50%), and the dips reproduce across runs. We do not interpret these dips mechanistically; they show that magnitude and Wanda, adapted to head pruning, give *unstable* orders, which is precisely why we report full sparsity curves rather than a single budget. The co-ablation orders are by contrast smoothly monotonic. Taylor is monotonic and far stronger than magnitude or Wanda, yet still trails co-ablation and collapses at 70%.

E.3 PERPLEXITY: CROSS-MODEL, FULL SWEEP

Table 27 extends the full perplexity sweep to the larger models. The self-repair-aware gain over the static co-ablation order grows with scale and sparsity: it is negligible on Pythia-1.4B (the static order is already near-optimal, and at 60–70% the two tie within noise), moderate on GPT-2-large (37 vs. 44 at 50%, 52 vs. 91 at 70%), and largest on Qwen-7B (54 vs. 91 at 50%, 240 vs. 1341 at 70%), consistent with larger models carrying more backup redundancy to preserve.

E.4 ZERO-SHOT ACCURACY ACROSS SPARSITIES

The main-text figure plots the three-seed accuracy curves of PIQA, ARC-Easy, and HellaSwag to 50%. Across every confirmed budget the co-ablation orders dominate magnitude, Wanda, and Taylor, which fall toward the chance levels (PIQA 50, ARC-E and HSw 25); the self-repair-aware order

Table 27: WikiText-2 perplexity across the full 10 to 70% head-sparsity sweep on three further scales, all six orders (Qwen-7B is also plotted in Figure 5c; GPT-2-small in (b)). Best per column in bold. Taylor needs a backward pass and exceeds memory on Qwen-7B in our environment. Co-ablation energy dominates every weight/magnitude/gradient baseline at every budget; the self-repair-aware order adds a further refinement that grows with scale and high sparsity, while on the small Pythia model the static order is already near-optimal and the two essentially tie.

order (PPL ↓)	10	20	30	40	50	60	70
<i>GPT-2-large</i> (dense 29.6)							
random	31	34	40	45	117	277	488
magnitude	30	32	38	51	77	124	184
Wanda	31	37	63	88	210	316	653
Taylor	30	33	36	41	45	55	78
co-abl. static	30	31	32	36	44	55	91
CoAX	30	31	32	34	37	42	52
<i>Pythia-1.4B</i> (dense 21.9)							
random	25	38	108	158	491	1155	1302
magnitude	23	24	28	78	178	217	459
Wanda	22	25	149	171	356	450	558
Taylor	23	24	26	31	41	55	99
co-abl. static	23	24	25	30	38	46	66
CoAX	23	23	25	29	35	47	73
<i>Qwen-2.5-7B</i> (dense 16.2)							
random	46	173	601	1195	7544	18298	119377
magnitude	49	66	123	29613	65157	80280	79277
Wanda	46	66	29709	66182	79750	80023	78816
Taylor	–	–	–	–	–	–	–
co-abl. static	20	27	31	50	91	426	1341
CoAX	21	24	29	35	54	92	240

helps or ties on every model-task cell, with seven of nine strict wins at 50%. That the conditional re-measurement never *hurts* accuracy, on any model-task cell, is the practical form of the paper’s claim: anticipating what a backup will do once its primary is gone can only sharpen a removal order, never coarsen it, so the self-repair-aware variant is a safe default rather than a tuned one.

E.5 MODULE-PARTITION NEGATIVE

Cutting the curvature graph into signed eigen-modules and pruning within-module does not beat flat second-order pruning (Qwen-2.5-7B at 30%: 29.4 versus 28.4 flat; both collapse by 50%), because flat pruning already accumulates the full off-diagonal interaction while a hard partition discards it. The graph’s compression value is in the self-repair-aware ranking, not a partition. We report this as a second honest negative.

E.6 CROSS-SCALE GEOMETRY

Table 28 gives the per-circuit cluster-AUC on GPT-2-small (the second-order/co-activation contrast in detail), and Table 29 gives the per-model VS-ACTIVE ROC-AUC behind Figure 18.

Pairwise synergy wins duplicate-token on 11/12 models (the exception is Pythia-1.4B) and previous-token on 10/12 (exceptions GPT-2-large and GPT-Neo-1.3B), while co-activation wins induction on all 12. The first-order co-ablation affinity shows the same qualitative split (output-side wins movement, loses induction) but is weaker on duplicate-token, so we report the second-order signal as the principled fixed choice. The reversals occur where the empirically-detected circuit is small or noisy, making the VS-ACTIVE split unstable; they are not concentrated at any scale. The pattern, output-grounded synergy for movement-by-output circuits and input-grounded co-activation for co-firing induction under repeated-token calibration, is the output-versus-input complementarity the paper argues for.

Table 28: **Cluster-AUC** (pair-level same-circuit, VS-ACTIVE) on GPT-2-small, mean over 4 seeds. **1st**: single-ablation affinity; **2nd**: pairwise synergy; **act**: co-activation; **wt**: projection-kernel weight subspace (Yamagiwa et al., 2026). Synergy wins on movement circuits over both input-side controls; co-activation wins co-located writing heads. This is the cluster-AUC, not the backup-AUC of Table 1 – the low backup-NM synergy entry is a same-circuit score, unrelated to the 0.91 backup-discovery result.

	dup-token	induction	prev-token	name-mover	neg-NM	s-inhib	backup-NM
1st (single)	0.88	0.73	0.68	0.34	0.98	0.62	0.43
2nd (synergy)	0.97	0.94	0.87	0.76	0.85	0.64	0.29
act	0.32	0.75	0.61	0.90	0.97	0.86	0.76
wt	0.59	0.89	0.73	0.79	0.96	0.74	0.79

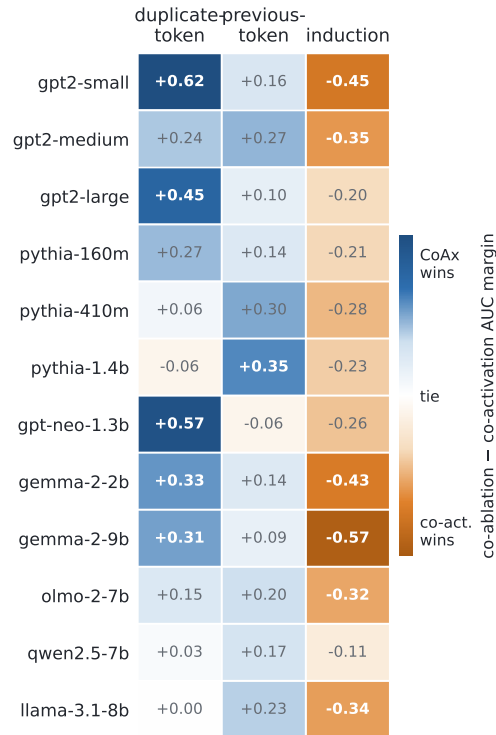


Figure 18: **Cross-scale, cross-architecture geometry across twelve models.** Each cell is the margin (co-ablation – co-activation VS-ACTIVE ROC-AUC) on a movement circuit: blue where the output-grounded co-ablation lens wins, orange where the input-side co-activation lens wins. The pattern is consistent across scale and architecture and is set by the circuit *mechanism*, not the model – co-ablation wins the output-movement circuits (duplicate-/previous-token) on 11/12 and 10/12 models, while co-activation wins induction on all 12, whose heads trivially co-fire under repeated-token calibration. This is a *same-circuit clustering* test, distinct from the conditional induction-completion experiment below; the induction reversal reflects co-firing, not a completion failure.

Table 29: Per-model movement-circuit VS-ACTIVE ROC-AUC. To avoid any per-cell signal selection, the co-ablation column (co) is a *single fixed* signal – the second-order pairwise synergy, the genuine contribution of this work – compared to co-activation (act), for duplicate-token (dup), previous-token (prev), and induction (ind). The winning lens in each pair is in bold. Pairwise synergy wins dup on 11/12 models (exception Pythia-1.4B) and prev on 10/12 (exceptions GPT-2-large and GPT-Neo-1.3B); co-activation wins ind on all 12 under repeated-token calibration.

model	dup		prev		ind	
	co	act	co	act	co	act
Pythia-160M	.65	.38	.56	.42	.43	.94
Pythia-410M	.62	.56	.66	.36	.53	.95
GPT-2-sm	.98	.37	.68	.52	.48	.94
GPT-2-md	.54	.46	.64	.39	.52	.98
GPT-2-lg	.84	.39	.60	.67	.79	.99
GPT-Neo-1.3B	.94	.37	.45	.77	.40	.97
Pythia-1.4B	.55	.61	.64	.28	.39	.83
Gemma-2-2B	.72	.43	.60	.46	.27	.87
OLMo-2-7B	.86	.71	.56	.36	.40	.86
Qwen2.5-7B	.65	.62	.41	.24	.71	.93
Llama-3.1-8B	.69	.68	.54	.31	.58	.92
Gemma-2-9B	.96	.65	.43	.40	.26	.89

F LIMITATIONS, BROADER IMPACT, AND REPRODUCIBILITY

F.1 LIMITATIONS

The explicit pairwise route is $O(|\mathcal{U}|^2)$, mitigated by candidate sets and the $O(|\mathcal{U}|)$ conditional route. Head-level backup ground truth exists mainly for GPT-2-small’s IOI circuit, so the labeled backup AUC is anchored there. This is a field-wide constraint rather than a quirk of our setup: the community’s hand-verified circuits remain a small set (IOI, induction, greater-than, docstring) (Wang et al., 2022; Conmy et al., 2023; Mueller et al., 2025), and only IOI documents *backup* heads specifically. We reduce – but do not eliminate – this single-circuit dependence three ways: a powered controlled-redundancy synthetic benchmark that supplies the head-to-head statistical comparison the eight documented backups cannot (Appendix C.1.4); the label-free completeness criterion, which validates the completed circuit without backup labels (§3.3); and label-free generalization on induction across scales and architectures. A second circuit with documented head-level backups would nonetheless strengthen the labeled evaluation, and none is currently available. The signal is instantiated primarily at attention-head granularity: it transfers to the attention-mediated induction circuit but not to the MLP-mediated greater-than circuit. A preliminary FFN-group probe (Appendix C.4.3) finds only weak recovery on greater-than, indicating it is weakly self-repairing at *both* head and FFN-group granularity – a property of the circuit, not of the unit. Conditional discovery is seeded by a primary set, and finding the primary components automatically is an open problem in its own right – automatic circuit discovery remains an active, unsolved area (Conmy et al., 2023; Mueller et al., 2025) and is further hampered here by the same self-repair that masks the backups. Three natural extensions follow: joint primary-and-backup discovery that breaks the masking on both sides at once; a full FFN-level treatment of strongly MLP-mediated self-repair (which greater-than lacks); and decomposing discovered backups into their known self-repair mechanisms (LayerNorm rescaling versus anti-erasure), of which our activation-ratio check is a first step.

F.2 BROADER IMPACT

COAX is an analysis tool for frozen models and trains nothing. By making redundant and backup components visible without labels, it can improve the faithfulness of interpretability audits and the safety of pruning, since a pruner unaware of backups can silently remove the components that keep a behavior robust. We see no direct path to misuse beyond that of interpretability methods in general.

F.3 ASSETS, LICENSES, AND ETHICS

All models are public pretrained checkpoints used under their respective licenses: GPT-2 and GPT-Neo (MIT), Pythia and OLMo-2 (Apache-2.0), Gemma-2 (Gemma Terms of Use), Llama-3.1 (Llama Community License), and Qwen-2.5 (Qwen License); we use them unmodified for inference-only analysis. Evaluation data are WikiText-2 (perplexity), the templated IOI prompts of Wang et al. (2022), and PIQA, ARC-Easy, and HellaSwag (zero-shot accuracy), each used through the standard lm-eval-harness under its public research license. No human subjects, private, or personally identifying data are involved; the IOI templates use common given names only.

F.4 REPRODUCIBILITY

All discovery and attribution experiments run on a single GPU in seconds to minutes (Table 6); the pruning sweeps to 70% on the 7B model are the most expensive, at a few GPU-hours, and no training is performed at any point. GPT-2-scale discovery (kernel build, conditional co-ablation, and all baselines) also runs on CPU in minutes, so the headline IOI results reproduce without a GPU. Experiments use a single 24 GB GPU; the 13B variants were out of scope for this budget. All weights are loaded frozen, and the random seeds for prompt sampling and ablation-value draws are fixed and listed in Table 8.